Revisiting the geographical extent of exceptional warmth in the Early Paleogene Southern Ocean

Joost Frieling[1], Steve Bohaty[2], Margot Cramwinckel[1], Tammo Reichgelt[3], Stephen Gallagher[4], Guy Holdgate[5], Francien Peterse[1], Jörg Pross[6], Appy Sluijs[1], and Peter Bijl[1]

[1]Utrecht University
[2]Heidelberg University
[3]University of Connecticut
[4]The University of Melbourne
[5]Geotrack International
[6]University of Heidelberg

November 23, 2022

Abstract

To assess zonal temperature and biogeographical patterns in the Paleogene of the Southern Ocean, we present new multi-proxy air and sea surface temperature data for the latest Paleocene (~57–56 Ma) and the Paleocene-Eocene Thermal Maximum (PETM; ~56 Ma) from the northern margin of the Australo-Antarctic Gulf (AAG). The various proxies document the well-known late Paleocene gradual warming and, superimposed, two late Paleocene pre-cursor warming events, hundreds of kyrs prior to the PETM. Remarkably, however, air and sea surface temperature reconstructions for the AAG and SW Pacific during the latest Paleocene, PETM and Early Eocene Climatic Optimum (~53–49 Ma) show similar trends and, within proxies, similar absolute temperatures. The record implies that the exceptional warmth previously recorded in the SW Pacific extended westward into the AAG. This contrasts with the modeled circulation and temperature patterns. We suggest that simulations of ocean circulation underestimate heat transport in the SW Pacific due insufficient resolution, not allowing for mesoscale eddy-related heat transport. We argue for a systematic approach to tackle model and proxy biases in marginal marine settings, including assessment of underexplored factors as high-latitude proxy mechanisms to confidently assess temperature in these non-analogue climates.

Revisiting the geographical extent of exceptional warmth in the Early Paleogene Southern Ocean

Frieling, J.[1§*], Bohaty, S.M.[2], Cramwinckel, M.J.[1], Gallagher, S.J.[3], Holdgate, G.R.[4], Reichgelt, T.[5], Peterse, F.[1], Pross, J.[2], Sluijs, A.[1], and Bijl, P.K.[1*]

[1] Department of Earth Sciences, Faculty of Geosciences, Utrecht University, Princetonlaan 8a, 3584CB, The Netherlands
[2] Institute of Earth Sciences, Heidelberg University, Im Neuenheimer Feld 234, D-69120 Heidelberg, Germany
[3] School of Geography, Earth and Atmospheric Sciences, The University of Melbourne, Melbourne, Australia
[4] Geotrack International, Brunswick West, Australia
[5] Department of Geosciences, University of Connecticut, Beach Hall, 354 Mansfield Road, Storrs CT 06269, USA

§Now at: Department of Earth Sciences, University of Oxford, South Parks Road OX1 3AN, UK
*Corresponding authors: Joost Frieling (joost.frieling@earth.ox.ac.uk), Peter Bijl (p.k.bijl@uu.nl)

Abstract

To assess zonal temperature and biogeographical patterns in the Paleogene of the Southern Ocean, we present new multi-proxy air and sea surface temperature data for the latest Paleocene (~57–56 Ma) and the Paleocene-Eocene Thermal Maximum (PETM; ~56 Ma) from the northern margin of the Australo-Antarctic Gulf (AAG). The various proxies document the well-known late Paleocene gradual warming and, superimposed, two late Paleocene pre-cursor warming events, hundreds of kyrs prior to the PETM. Remarkably, however, air and sea surface temperature reconstructions for the AAG and SW Pacific during the latest Paleocene, PETM and Early Eocene Climatic Optimum (~53–49 Ma) show similar trends and, within proxies, similar absolute temperatures. The record implies that the exceptional warmth previously recorded in the SW Pacific extended westward into the AAG. This contrasts with the modeled circulation and temperature patterns. We suggest that simulations of ocean circulation underestimate heat transport in the SW Pacific due insufficient resolution, not allowing for mesoscale eddy-related heat transport. We argue for a systematic approach to tackle model and proxy biases in marginal marine settings, including assessment of underexplored factors as high-latitude proxy mechanisms to confidently assess temperature in these non-analogue climates.

Introduction

Periods of transient warming superimposed on sustained greenhouse climates during the Paleocene and Eocene (early Paleogene; ca. 66–34 Million years ago (Ma)) may be employed as potential analogues for current climate change and potential end-member climate states under unabated carbon emissions (Burke et al., 2018). A negative carbon isotope excursion (CIE), globally recorded in terrestrial and marine sediments, combined with ocean acidification (Zachos et al., 2005; McInerney and Wing, 2011) at the onset of the Paleocene-Eocene Thermal Maximum (PETM; 56 Ma) shows the rapid input of thousands of petagrams of ^{13}C-depleted C to the exogenic carbon pool (Dickens et al., 1995), providing a geologic analogue to present-day anthropogenic emissions. Several similar, smaller, events appear to have occurred in the late Paleocene and throughout the early Eocene (Cramer et al., 2003; Lauretano et al., 2015; Westerhold et al., 2020) although their climatic expression remains unknown.

In recent years, fully coupled climate models have been able to broadly reproduce sea surface and air temperature proxy data for the warmest periods of the Cenozoic (Cramwinckel et al., 2018; Evans et al., 2018; Lunt et al., 2021). Similarly, the models can reproduce the magnitude of extreme transient warming across the PETM (Dunkley Jones et al., 2013; Frieling et al., 2017; Hollis et al., 2019; Zhu et al., 2019; Lunt et al., 2021). This suggests that such models provide accurate reflections of global climate states and meridional gradient changes under high radiative forcing. However, even in simulations where the majority of the reconstructed sea surface temperature (SST) patterns and deep ocean temperatures are consistent with model output throughout the Eocene, absolute temperature reconstructions from several regions, notably the Arctic and the SW Pacific Ocean, and in particular the area around the Tasman Gateway and Zealandia, are still much (>10 ºC) warmer than simulations (Frieling et al., 2017; Cramwinckel et al., 2018; Evans et al., 2018; Lunt et al., 2021). In contrast to the reconstructions showing exceptional regional warmth, the Southern Ocean, including the south Pacific Ocean, was likely the dominant locus of cold deep-water formation during much of the Paleogene (Pak and Miller, 1992; Huck et al., 2017), highlighting the importance of resolving the paleoceanography and mechanistic understanding of the enigmatic warmth in and around the SW Pacific (Bijl et al., 2009; Hollis et al., 2009; Douglas et al., 2014).

SST estimates from the SW Pacific and the Antarctic margin of the Australo-Antarctic Gulf (AAG) (Figure 1) both consistently exceed 30 ºC, and megathermal vegetation elements were established during the PETM and early Eocene climate optimum (EECO; ~53–49 Ma) (Bijl et al., 2009; Sluijs et al., 2011; Carpenter et al., 2012; Pross et al., 2012; Bijl et al., 2013a; Contreras et al., 2013; Contreras et al., 2014; Hollis et al., 2015; Bijl et al., 2021; Huurdeman et al., 2021; Reichgelt et al., 2022). Moreover, dinoflagellate cyst (dinocyst) biogeography suggests surface circulation dominated by low and high latitude-derived current influence in the AAG and SW Pacific (Fig. 1a), respectively (Bijl et al., 2011; Bijl et al., 2013b). These interpretations are broadly supported by modeling efforts (Huber et al., 2004) and such a regional circulation pattern results in consistently higher modeled SST in the northern AAG compared to the southwest (SW) Pacific (e.g. Hollis et al., 2009, Fig. 1b). It is noteworthy that although proxy-derived SSTs for the SW Pacific are >10 ºC higher than the model-derived SSTs (e.g. Lunt et al., 2021) during the EECO, mean annual air temperature (MAAT) reconstructions can be matched by current models (Lunt et al., 2021; Reichgelt et al., 2022).

Regional paleoceanography, especially the gradual opening of the Tasman Gateway (TG), would have affected regional temperature trends through re-routing of warm *versus* cold ocean currents (Cande and Stock, 2004; Bijl et al., 2013a; Sijp et al., 2014; 2016). Recent efforts to constrain the consequence of gradual gateway opening suggest that the regional climatic impact of both the Drake Passage and Tasman Gateway is limited unless both allow relatively deep throughflow simultaneously (Sauermilch et al., 2021), a situation that does not seem to have occurred until *ca.* 26 Ma (van de Lagemaat et al., 2021). Therefore, even if a shallow connection existed during the Paleocene and early Eocene (Bijl et al., 2013a), it should have had a negligible impact on paleoceanography and heat transport. On the other hand, in very high resolution model simulations (<1º), warm mesoscale eddies reach further south than any current in low-resolution runs, resulting in substantial differences in modeled surface water temperatures in parts of the SW Pacific. Such oceanographic features can presumably reduce the temperature difference between the SW Pacific and the AAG directly surrounding the TG (Nooteboom et al., 2022).

Unfortunately, however, no well-dated temperature proxy or biogeographical data from the northern margin of the AAG, presumably the warmest place in this region, are available for some key intervals of the Paleogene; the latest Paleocene (*ca.* 57–56 Ma) and the PETM. These periods, along with the EECO, deserve particular attention as they are targeted by community data-model comparison efforts such as DeepMIP (Lunt et al., 2017; 2021 Hollis et al., 2019). However, the absence of data hampers the comparison of temperature on both sides of the Tasman Gateway, the reconstruction of regional oceanography and establishing a regional temperature response pattern. Consequently, in-depth assessment of model performance is limited, which is crucial in light of the apparent proxy-model mismatch.

To fill this data gap, we present new multi-proxy SST and MAAT estimates for two expanded late Paleocene-PETM sedimentary archives from the AAG at ~60ºS paleolatitude (Otway Basin, Victoria, Australia, Fig. 1) (Frieling et al., 2018); Huurdeman et al. 2021). Temperature estimates for the AAG are paired with previously published data from the SW Pacific to assess temperature differences across the Tasman Gateway (Table 1). To reconstruct temperature, we applied novel and established lipid biomarker proxies and palynological tools. We reconstruct MAAT from branched glycerol monoalkyl glycerol tetraethers (brGMGTs) (Baxter et al., 2019; Naafs et al., 2018), the relative abundance of isoprenoid glycerol dialkyl glycerol tetraethers (isoGDGTs) with 5 cyclopentane moieties (GDGT-5) (Naafs et al., 2018), and combine this with new and published nearest living relative (NLR)-based MAAT estimates from pollen and spore assemblages and branched GDGTs (brGDGTs) (Huurdeman et al., 2021). Furthermore, we applied the TEX_{86} to estimate (sub-)surface temperature (Schouten et al., 2002; Kim et al., 2010) and support sea temperature reconstructions by utilizing relative abundances of crenarchaeol-isomer to total crenarchaeol (f(cren ')) (Sinninghe Damsté et al., 2012; O'Brien et al., 2017; Bale et al., 2019). Dinocysts produced by thermophilic dinoflagellates and mangrove palm pollen were used to acquire minimum temperature thresholds.

Materials and Methods

Material and Setting

Samples from the Latrobe-1 core (38º 41' 35" S, 143º 09' 00" E) and the Point Margaret outcrop (~3 km east; 38º 43' 28.8" S, 143º 10' 35" E) were analyzed. A

description of sample collection, lithology and stratigraphy of the section was outlined in Frieling et al., (2018).

We focused on the latest Paleocene and PETM (Frieling et al., 2018), and analyzed a total of 114 samples for GDGTs and brGMGTs; 94 for Point Margaret and 20 for the Latrobe-1 core. Detailed dinocyst assemblage data were generated for 90 samples from Point Margaret and 20 samples from the Latrobe-1 core. For the latest Paleocene and PETM, brGDGT-based MAAT estimates were published in Huurdeman et al., (2021). The analyses performed for Huurdeman et al. (2021) were used for isoGDGTs and brGMGTs here.

The sites are represented by shallow-marine deposits, marked by a gradual up-section transition from (pro-)deltaic muddy sandstones to sandy silt and mudstones. The input of terrestrial organic matter, presumably from acidic soils and peats in the hinterland based on the consistent presence of *Sphagnum*-like spores and low brGDGT-based pH, is clearly dominant over marine sources in most section intervals (Frieling et al., 2018; Huurdeman et al., 2021). Sediments were deposited in a subsiding trough system, allowing for rapid and almost continuous sediment accumulation during continental rifting (Sauermilch et al., 2019).

The regional oceanography of the SW Pacific in the early Paleogene is thought to be characterized by the Antarctic-derived Tasman Current (TC) in the southernmost sector (Figure 1a, Huber et al., 2004; Bijl et al., 2011; Sauermilch et al., 2019 and references therein). Further north, the influence of the lower-latitude Proto-East Australia Current (PEAC) becomes pronounced. The low latitude Proto-Leeuwin Current (PLC) entered the AAG in the west and extended progressively further east as the AAG widened during the Cenozoic.

Palynology

A minimum of 200 and 300 specimens were determined to the species level for dinocysts and terrestrial palynomorphs, respectively, in the palynological materials described by Frieling et al. (2018). Dinocyst taxonomy follows Williams et al., (2017) except for the subfamily Wetzelielloideae, where we follow Bijl et al., (2016). We refer to Huurdeman et al. (2021) for details of the pollen and spore taxonomy. Pollen and spore assemblages of 7 samples from the Latrobe-1 bore and 61 from Point Margaret were used to generate NLR data following methodology as described in (Huurdeman et al., 2021). The occurrence and abundance of temperature-sensitive dinocyst and pollen taxa, including the dinocyst taxa *Apectodinium* spp. (>20 ºC) and *Florentinia reichartii* (>25 ºC) (Frieling and Sluijs, 2018), as well as the mangrove palm *Nypa* pollen (Reichgelt et al., 2018; Huurdeman et al., 2021) are used as quantitative thresholds to support minimum SST and MAAT constraints, respectively.

Organic geochemistry

We quantified isoprenoid and branched GDGT and brGMGT abundances from the ultra high performance liquid chromatography – mass spectrometry (UHPLC-MS) analyses conducted by Huurdeman et al., (2021). For a detailed description of the organic geochemistry methods and brGDGTs, we refer to Huurdeman et al. (2021). In short, a synthetic C_{46} standard (*m/z* 744) was added to obtain absolute concentrations. A minimum peak area cut-off (3000 units) was applied for individual components, which here typically amounts to absolute concentrations well below 1 ng g^{-1} dry sediment or ~10 µg g^{-1} TOC.

Mean Annual Air Temperature proxies & brGMGTs

In addition to the MAAT estimates based on brGDGTs and nearest living relative (NLR) from pollen and spore assemblages, which follow the approach described in Huurdeman et al. (2021), we here analyze brGMGT distributions. BrGMGTs are produced by unknown bacteria, and are characterized by an additional covalent C-C bond linking their two alkyl chains (Morii et al., 1998; Schouten et al., 2008). The presence of this bond is thought to improve the stability of the membrane under extreme environmental conditions, such as higher temperature. We identify brGMGT compounds with molecular masses of 1048, 1034 and 1020. In addition to peats (Naafs et al., 2018a) and lake sediments (Baxter et al., 2019), these compounds are also produced and recorded in the marine realm (Liu et al., 2012), particularly in oxygen-minimum zones (Xie et al., 2014). Following the outline in (Sluijs et al., 2020), we use the nomenclature of (Baxter et al., 2019) to identify the compounds utilized by the brGMGTI and HMBT-acyclic (Naafs et al., 2018a). The deep-time application of these indices and the abundance of brGMGTs relative to brGDGTs is explored further here (Fig. 2, Fig. S4-6).

We further estimate the abundance of isoprenoid GDGT-5, as a percentage relative to GDGT1-3. The occurrence of GDGT-5 (>1%) is restricted to regions with MAAT of at least 19 ºC in present-day acidic peats, a relation that has been applied to Paleogene lignites (Naafs et al., 2018b).

Sea surface temperature proxies

Prior to calculating TEX86 values, we test whether isoGDGTs generally align with those observed for the global core-top database of (Kim et al., 2010). Deviation from the core-top data would be indicated by high delta ring index (ΔRI) values (Zhang et al., 2016), implying the standard core top TEX_{86} calibrations may not yield reliable results. For samples that passed the ΔRI cut-off (<0.3), GDGT-2 over 3 ratios (hereafter [2/3]) are employed to assess whether a substantial fraction of GDGTs were deep-water derived (values above >5, see also Discussion).

To gain insight into SST trends from samples with substantial overprints, we employ f(cren') (Sinninghe Damsté et al., 2012; O'Brien et al., 2017; Bale et al., 2019; Baxter et al., 2021). Crenarchaeol is exclusively produced by Thaumarchaeota (Sinninghe Damsté et al., 2002; De La Torre et al., 2008) and therefore substantially less sensitive to overprints by methanogenic or methanotrophic archaea. In addition, Weijers et al., (2006) already noted that the relative abundance of crenarchaeol in soils is relatively low and decreases with increasing acidity; crenarchaeol rarely exceeds a relative abundance of 10% in acidic soils (pH <6). The same applies to peats and Paleogene lignites, where crenarchaeol rarely exceeds 5% (Naafs et al., 2018; Naafs et al., 2017b). Based on the cyclisation of brGDGTs (quantified in the CBT' index; De Jonge et al., (2014)), we find that soils with low pH (values <5 in Paleocene, ~5.5 during the PETM) dominate the distribution at our site (Huurdeman et al., 2021). Collectively, despite high BIT, the brGDGTs appear predominantly derived from acidic soils and peats which makes it likely that the majority of crenarchaeol in our samples is derived from marine Thaumarchaeota and not soils (Fig. S8). We therefore propose that f(cren') may provide supporting information on relative SST changes in setting with very high terrestrial GDGT input (Frieling et al., 2018; Huurdeman et al., 2021) based on the link between temperature and f(cren') in cultures as well as the modern core-top calibration dataset (Schouten et al., 2002; Kim et al., 2010; Tierney and Tingley, 2015; Bale et al., 2019). In the core-top data, SST explains a substantial part of the variability in f(cren') (linear $R^2 = 0.6$) in waters with an SST above 10 ºC, although this is slightly less than the traditional TEX_{86} (linear R^2

= 0.75) in the same dataset (Schouten et al., 2002; Tierney and Tingley, 2015)(Fig. S1). The basis of temperature dependency of f(cren') may be the result of membrane adaptation within Thaumarcheota populations, as the stereoisomer results in slightly different membrane packing (Schouten et al., 2013; Sinninghe Damsté et al., 2018; Bale et al., 2019). In the natural environment, the temperature dependency may also originate from shifts in the Thaumarcheotal populations as has been observed in lacustrine records (Baxter et al., 2021). In the latter case, the positive temperature correlation may come from more dominant (sub-)surface dwelling Thaumarchaeota group I.1b (proportionally high cren') relative to group I.1a (proportionally low cren'), for example due to changing oxygenation, stratification or nutrient distribution within the water column (Baxter et al., 2021). However, strains of Thaumarchaeota group I.1b have so far not been detected in the marine environment. Regardless of the exact mechanism, at nearby ODP Site 1172 (Sluijs et al., 2011; Bijl et al., 2021), virtually all variation in TEX_{86} is captured (R^2 = 0.98; Fig. S3) by f(cren') across the PETM. Together with the correlation to TEX_{86} and SST in the modern core-top dataset, this gives confidence that we can here use f(cren') to trace SST trends, albeit without coupling this to absolute SST values.

Data compilation for the Southern Ocean

We focus on late Paleocene, PETM and EECO marine and terrestrial temperature proxy records for the Southern Ocean, ranging from New Zealand in the southwest Pacific Ocean in the east, towards the AAG in the west, between paleolatitudes of 50º S and 65º S (Seton et al., 2012; Müller et al., 2019) (Fig. 1, Table 1). Both quantitative (GDGT-based proxies, foraminiferal Mg/Ca, NLR-based estimates) and semi-quantitative / qualitative (temperature-indicative dinocyst and mangrove palm pollen) temperature information is incorporated. Absolute temperatures are compared within proxies, within the selected time slices. Time-slices “latest Paleocene” (57–56 Ma) and “PETM” (~55.9 Ma) were identified based on carbon-isotope data ($\delta^{13}C$) if available (i.e., for ODP Site 1172 and DSDP Site 277) and/or on pollen-based biostratigraphy. We here use records from the upper *Lygistepollenites balmei* zone and the *Spinizonocolpites prominatus* subzone to represent the latest Paleocene and PETM, respectively. Consequently, the included Paleocene data have an maximum age of ~57 Ma (Frieling et al., 2018), in compliance with previous compilations and DeepMIP (Dunkley Jones et al., 2013; Frieling et al., 2017; Hollis et al., 2019). Only data comprising the ‘body’, the stable period of anomalously low $\delta^{13}C$ within the PETM CIE were used, in order to focus on the period of sustained peak warmth. Consequently, the rapid onset and more gradual recovery of the CIE, i.e., with $\delta^{13}C$ values, and potentially temperature, intermediate between background and peak PETM values, were not included. A broad interval covering the EECO, *ca.* 53–49 Ma, as defined by (Westerhold et al., 2018) previously identified by bio-, magneto- and isotope stratigraphy is used for the EECO data compilation (Hollis et al., 2019). As it is often challenging to assign absolute ages for terrestrial deposits, we also include localities that were determined to be “Ypresian” and “Early Eocene” in age (Hollis et al., 2019).

Results

Mean annual air temperature estimates for the northern Australo-Antarctic Gulf

BrGDGTs

Distributions of brGDGTs in sediments from Point Margaret are generally indistinguishable from those in modern soils and peats, with negligible riverine or marine sedimentary contributions throughout the entire succession (Huurdeman et al. 2021 and supplement thereof). We here extended the brGDGT-based MAAT estimates for the entire late Paleocene part of the Point Margaret section (Fig. 2). There is a long-term warming trend (~4 ºC) from ~18 ºC to 22 ºC from the top of the section to the onset of the PETM warming around 50.8m. We find two minor pre-cursor warming events around ~33 m and 46 m, also supported by other proxies (NLR, f(cren'), dinocysts), superimposed on the long-term trend. Potentially similar fluctuations further down section (e.g. ~27 m, Fig. S9) in brGDGT-based MAAT cannot be confirmed as warming events as these fluctuations are not mimicked by similar signals in other proxies.

Isoprenoid GDGT-5

In the Point Margaret sediments we find abundant GDGT-5. The occurrence and abundance of this compound in our shallow marine setting is likely explained by substantial input of peat-derived material, consistent with the presence of *Sphagnum* spores (Huurdeman et al. 2021). Although there is substantial scatter and a few (n = 13) samples without GDGT-5 throughout the section, GDGT-5 is mostly present (n = 81) and comprises up to ~10% of the isoGDGT assemblage (GDGTs 1-3), close to the maximum percentage observed for modern tropical peats (Fig. 2, Fig. S9). In the upper part of the section, %GDGT-5 reaches a maximum of 3% on a relatively stable latest Paleocene (43-50m height) average ~1.5%. In this interval, %GDGT-5 appears to broadly follow brGDGT-derived temperatures.

However, as GDGT-1 to 3, used to calculate %GDGT-5, are also derived from marine Thaumarcheota and possibly other non-terrestrial sources (Fig. S4, S8), the calculated %GDGT-5 for all our samples must be regarded as a minimum estimate of the original source. Considering the calculated terrestrial fraction of GDGT-1 to 3 is ~30-50% (Supp. Data) in some late Paleocene intervals, the relative abundance of GDGT-5 in the source material could well have been similar to, or higher than some modern tropical peats (Naafs et al., 2018). A single-point within the body of the CIE reaches ~6% GDGT-5 (Fig. 2E). However, it is difficult to gauge the value of this observation: starting from the onset of the CIE, %GDGT-5 and *Sphagnum* spores are no longer consistently present, implying that most of the source material is lost, or at least does not always reach the site.

BrGMGTs

The Point Margaret section yields a suite of brGMGTs that have recently been documented in peats (Naafs et al., 2018a), Paleogene lignites (Naafs et al., 2018a), and African lakes (Baxter et al., 2019) and both modern marine surface (Liu et al., 2012) and Paleogene marine sediments (Sluijs et al., 2020; Bijl et al., 2021). Naafs et al. (2018a) show that the relative abundance of brGMGTs over regular brGDGTs is positively correlated with MAAT in peats. In the Point Margaret section, the amount of brGMGTs relative to brGDGTs is positively correlated to MBT'$_{5Me}$-based MAAT, but is marked by higher values (>10% of total brGDGTs) than all modern peat samples at the same MAAT (Fig. S5). This may signal that we significantly underestimate absolute temperatures or that additional sources, for example marine (sedimentary) organisms, add brGMGTs in our setting (Baxter et al., 2021; Kirkels et al., 2022). Baxter et al. (2019) calibrated the brGMGT distributions, formulated as the brGMGT-index (brGMGTI), in tropical lake sediments to temperature. Although the

application of the brGMGTI proxy outside tropical lakes is unvalidated, we note that the brGMGT-derived MAAT response at our site is somewhat greater than that based on regular brGDGTs (Fig. 2D). We also find high scatter in this proxy in some intervals (particularly around the onset of the PETM CIE, 49-51m), which may suggest the mixing of different brGMGT sources, likely peat and *in situ* marine.

Despite the relatively limited range of temperature covered in our data, the HMBT-acyclic (Naafs et al., 2018a) shows a strong correlation with e.g. MBT'$_{5Me}$ and f(cren') (Fig. S7, Supp. Text). However, accurately assigning variability to either air or sea surface temperature, or another, indirect control is difficult without proper source identification (Kirkels et al., 2022). Collectively, it is noteworthy that both HMBT-acyclic and brGMGTI follow MBT'$_{5Me}$ MAAT trends and that brGMGTI produces similar MAAT despite the lack of an environment-specific calibration.

Terrestrial palynomorphs and NLRs

The expanded late Paleocene record (0–47m) yields relatively high MAAT (~18 ºC) considering its paleolatitude between 55 and 65º S. These late Paleocene NLRs of the pollen and spore taxa align well with estimates from the upper part of the Point Margaret section (Huurdeman et al. 2021) and Latrobe-1 (this study). NLR-based MAATs are 17–19.8 ºC (median: 18.1 ºC) for the late Paleocene. MAAT estimates from the lower part of the section (2–30m) yield values around 17ºC, and slightly higher (~18ºC) in the upper part of the succession (30–48m), with subtle increases signaling pre-cursor warming events (~33m and ~46m) also observed in brGDGT-based MAAT estimates. A ~3–4 ºC rise in MAAT was previously calculated for the PETM (Huurdeman et al. 2021).

Aside from the nearest living relative approach to estimate MAAT, we use the well-known climatic envelopes of fossil pollen taxa such as *Spinizonocolpites prominatus* (*Nypa*), a mangrove palm that only occurs in regions with MAAT >22 ºC at present (Reichgelt et al., 2018). This species has a first consistent appearance at 50.57 m at Point Margaret (Fig. 2F), 23 cm below the CIE onset (Huurdeman et al., 2021), and occurs within the PETM CIE body (299.67 m below surface) and the EECO in the Latrobe-1 core (Frieling et al., 2018). The presence of *Nypa* implies that coastal MAAT was at least 22 ºC in the northern AAG just prior to and during the PETM and during the EECO.

Sea surface temperature estimates for the northern Australo-Antarctic Gulf

TEX_{86}

We generated new isoGDGT data for the Point Margaret outcrop and Latrobe-1 borehole. The isoGDGT distributions in most samples from the Point Margaret section and the Latrobe-1 bore have ΔRI values >0.3 signaling non-pelagic contributions to the isoGDGT pool (Zhang et al., 2016). In most samples, soil-derived isoGDGT input, as indicated by the branched and isoprenoid tetraether (BIT) index and contributions from methanogenic and methanotrophic isoGDGT producers, as derived from the Methane Index (MI) exceeded generally proposed cut-offs (0.3–0.4 for BIT (Hopmans et al., 2004; Weijers et al., 2007) and 0.3 for MI (Zhang et al., 2011)). Concentrations in the Latrobe-1 samples are <1 ng g^{-1} sediment or <10 mg g^{-1} total organic carbon (TOC) for most compounds, generally sufficient to identify, but not properly quantify, isoGDGTs, and insufficient to identify penta- and hexamethylated brGDGTs and brGMGTs. This implies that brGDGT distributions could not be used to estimate mean annual air temperature for these samples. We also note that the recorded concentrations are remarkably low compared to the sediments

from the nearby (~3 km) Point Margaret, which may be the result of oxidation during long-term (40–50 year) dry storage. A similar effect was noted for dinocysts (Frieling et al., 2018).

Excluding samples with high ΔRI, only 5 samples at Point Margaret were identified as suitable to calculate TEX_{86}-derived SST, of which 4 are from the PETM CIE. A single late Paleocene data point with ΔRI <0.3 yielded a TEX_{86} value of 0.66, and although this sample does pass the ΔRI cut-off, it is marked by a very high BIT index value (0.76). Similarly, two late Paleocene high-BIT index samples from the Latrobe-1 core with low GDGT-3 abundances (<3000 peak area, typically <0.5 ng g^{-1} sediment for GDGT-3), had otherwise normal isoGDGT-distributions based on ΔRI values (<0.3) and yielded TEX_{86} values of 0.67. However, as the concentrations of most isoGDGTs and brGDGTs approach the analytical limits and potentially have high terrestrial isoGDGT contributions, the resulting TEX_{86} values must be viewed with caution as the analytical error is larger than for other samples and indices. Absolute SST estimates based on TEX_{86}^{H} (Kim et al., 2010) are ~27 ºC for the late Paleocene and ~32 ºC during the PETM, implying a 5–6 ºC warming during the PETM.

f(cren')

In the Point Margaret section, we further constrain the temperature trends in the marine realm using the fractional abundance of the crenarchaeol stereoisomer relative to total crenarchaeol (f(cren')) (Fig. 2B). Similar to the data from ODP 1172, in Point Margaret, f(cren') shows a strong linear relation with the scarce TEX_{86} data (R^2 = 0.96, p = 0.002, n = 5) and broadly reproduces the long-term rise in brGDGT- and NLR-derived temperatures in the late Paleocene (0–50 m), as well as the two late Paleocene transient precursor warming episodes (~33 and 46m) (Fig. 2B, 2F). The precursor warming events are pronounced in f(cren'), whereas the response in brGDGTs and NLR appears more subdued.

Moreover, f(cren') rises just before (50.57 m) the onset of the CIE (50.8 m), whereas the rise in MBT'_{5Me} slightly lags the CIE (~51 m). SST rise directly prior to the CIE, as recorded here in f(cren'), has also been recognized elsewhere (Thomas et al., 2002; Sluijs et al., 2007; Secord et al., 2010; Frieling et al., 2019). The presumed temperature signal obtained from f(cren') is supported by the coeval appearance of mangrove palm pollen (Huurdeman et al., 2021, Fig. 2F). The delayed response (up to a few kyr) in brGDGT-based MAAT compared to vegetation-derived MAAT was attributed by Huurdeman et al. (2021) to 1) differences in transport time and/or 2) reworking of Paleocene or even older soil materials (John et al., 2012) and clay-bound organics (Schneider-Mor and Bowen, 2013), including brGDGTs. This may result in an apparent delay in warming in peat and soil-derived components (brGDGTs, and (peat-derived) brGMGTs) while warming based on above ground vegetation (palynomorphs), especially coastal elements (mangrove palms) and marine compounds (f(cren'), dinocysts), would be more synchronous with the warming. It might be these processes also played a role in suppressing the temperature change inferred from brGDGTs relative to other proxies during the precursor warming events.

Dinocysts

Late Paleocene and PETM SST trends as reconstructed through f(cren') are supported by progressively higher percentages of thermophilic dinocysts towards the top of the

Paleocene section (Fig. 2C), even though these taxa are outnumbered by low-salinity tolerant taxa during pre-CIE warming and onset of the PETM CIE (*ca.* 50–50.9 m, Fig. S9). In addition to rough trends, the appearance and relative abundance of selected extinct thermophilic dinocysts, notably *Apectodinium* spp. and *Florentinia reichartii* provide constraints on minimum SST. The first abundance events of *Apectodinium* (>10%) are found during the precursor warming events in the latest Paleocene (at ~33 m and ~46 m, Fig. 2C) at Point Margaret. These events are not registered in the Latrobe-1 core, which may be due to low sampling resolution and/or poor recovery in the respective core intervals. A third abundance increase is recorded at Point Margaret during the CIE, which is mirrored by a similar event in the Latrobe-1 core (SI; Fig. S10). *F. reichartii* is never abundant (maximum: 5% at Point Margaret), and occurs consistently only during peak CIE. A single late Early Eocene (EECO) abundance event of *Apectodinium* is found in the Latrobe-1 core (pers. obs. J. Frieling). Following observations of Frieling and Sluijs, (2018) we arrive at most likely minimum SST estimates ~20–25 ºC for the latest Paleocene (based on occasional *Apectodinium* abundance; Latrobe-1 core and Point Margaret), 25–30 ºC for the PETM (based on *F. reichartii*) for the Point Margaret section and 20–25 ºC for the EECO in the Latrobe-1 core. The relative abundance of these thermophilic taxa follows the long-term late Paleocene SST rise, as well as short-term variations (Fig. 2) observed in other temperature proxies (f(cren'), MBT'_{5Me}, brGMGTI) in detail except for a short interval around the CIE onset at Point Margaret.

Integrated regional SST for the AAG and SW Pacific (Table 1)

The early Paleogene climate of the SW Pacific has been intensely studied with a range of proxies (Hollis et al., 2019). The majority of SST data is based on TEX_{86}, and secondly planktonic foraminiferal Mg/Ca ratios. Briefly, the SW Pacific TEX_{86}^{H} and Mg/Ca records show SSTs of ~26–30 ºC in the late Paleocene (Table 1), rising to 31–33 ºC during the PETM. For the EECO, results are somewhat more variable and carbonate-based proxies show somewhat lower temperatures on average (~26 ºC) compared to TEX_{86}^{H} (31–32 ºC) (Hollis et al., 2019).

Fewer data were available for the AAG and prior to this study, none for the late Paleocene and PETM. Although some caution is warranted due to high BIT in our samples, the new data suggest that TEX_{86}-based SSTs in the late Paleocene (27 ºC), PETM (~32 ºC) and the published data from Site U1356A (32 ºC) were indistinguishable from those in the SW Pacific in the same intervals.

This is supported by semi-quantitative lines of evidence, particularly the occurrence and abundance of thermophilic dinocysts; the abundance of *Apectodinium* and occurrence of *F. reichartii* during the PETM are mirrored east and west of the Tasman Gateway (Figure 3, 4). Similarly, high SSTs during the EECO of U1356 are accompanied by high relative abundances of *Apectodinium*.

Integrated regional mean air temperatures for the AAG and SW Pacific (Table 1)

For the SW Pacific, MAATs have been reconstructed for several localities, but, due to the nature of the proxies, a relatively small number of samples per location compared to SSTs. Available Late Paleocene MAAT reconstructions for the SW Pacific region are mostly vegetation-based (e.g. NLR, leaf margin analyses) approaches. This includes localities Konkon-1 and Poonboon-1 in the Bass Basin (e.g. Contreras et al., 2014), and Cambalong Creek, on the southeast Australian coast (Greenwood et al., 2003) (Fig. 1), ODP Site 1172 and Mid-Waipara, New Zealand, which together arrive

at an average of ~16 ºC, with MAAT rising to ~20 ºC during the PETM. The EECO MAAT estimates are based on brGDGT-based proxy applications from ODP Site 1172 (Bijl et al., 2013a; Bijl et al., 2021) and Mid-Waipara (Pancost et al., 2013), and yield MAAT of ~21-22 ºC.

Within the AAG realm, late Paleocene MAAT reconstructions are now available for the Point Margaret outcrop (Huurdeman et al., 2021; this study) and Latrobe-1 (this study). The abundance of GDGT-5 in the latest Paleocene of the Point Margaret outcrop indicates MAAT >19 ºC, the NLR-based estimates (Latrobe-1 & Point Margaret) arrive at 16–19 ºC and the Point Margaret brGDGT-based estimates are 21-22 ºC. Both NLR and MBT'$_{5Me}$ indicate a MAAT rise during the PETM, to 20–22ºC and 23ºC, respectively. BrGMGTI derived MAAT estimates suggests slightly higher temperatures during the PETM (~24 ºC) and a temperature increase comparable to NLR-based estimate (~4 ºC), although these results should be treated with some caution, as brGMGTI estimates were only calculated for Point Margaret and this novel proxy remains largely untested. MAAT estimates for the EECO are derived from only few localities (Table 1). This includes Lowana Road, also known as Regatta Point, in the Sorrell Basin, western Tasmania, IODP Site U1356A on the Antarctic Margin and two recent ensemble (NLR and leaf-morphology) estimates from Dinmore and Deans Marsh, Australia (Reichgelt et al., 2022). The localities show somewhat divergent plant-based MAAT estimates; NLR shows MAAT ~18 ºC at U1356A, while a higher MAAT is reconstructed for Lowana Road (~24ºC). The ensemble MAAT estimates from Dinmore and Deans Marsh fall between these estimates. BrGDGT-based estimates from U1356A align with the average of all vegetation-based estimates (~20–21 ºC). Similar to the SST estimates, MAAT estimates from the SW Pacific and AAG within the same proxy are indistinguishable for the same intervals.

Terrestrial micro- and macrofossil evidence paint a very similar picture: mangrove palm pollen (*Nypa*) are found throughout the entire studied area during the PETM (Fig. 4) and also appear during the EECO (e.g. Latrobe-1 core (J. Frieling pers. obs.) and Lowana Road (Carpenter et al., 2012)).

Discussion

Late Paleocene warming events

Multiple temperature proxies reflect two late Paleocene transient warming events superimposed on subtle long-term warming (Fig. 2). These events do not seem to be local. The second pre-cursor warming (PW-2) at ~46m in the Point Margaret section has an equivalent at ODP Site 1172 (Fig. 3). This may also hold true for the event at ~33m, although at ODP Site 1172 only very subtle increases in *Apectodinium* abundance (~613.2 and ~615.5 m below sea floor) are found (Bijl et al., 2021). Based on average late Paleocene accumulation rates at ODP Site 1172 (0.6 cm kyr^{-1}; Sluijs et al., 2011) and Point Margaret (average ~7 cm kyr^{-1}; Frieling et al., 2018), PW-2 may precede the PETM by some 100 kyr, and by extrapolation, this would imply PW-1 at 33m is perhaps another ~200 kyr older but we note that in marginal settings sedimentation rates can strongly vary on short time-scales. Although their exact timing remains unclear, this is an interval in which only minor deep ocean carbon isotope fluctuations occur (Cramer et al., 2003; Westerhold et al., 2018; Westerhold et al., 2020). Given current constraints on their age, PW-1 and 2 appear to precede previously recognized precursor carbon isotope events that occur much closer to the PETM CIE (e.g. Bowen et al., 2015; Babila et al., 2022). Although it may be argued a

subtle decrease in $\delta^{13}C_{org}$ co-occurs with the precursor warmings, this could also result from coeval small changes in organic matter sourcing. We hence find no solid evidence for any CIE occurring at the same level as either of the transient precursor warming events.

However, even if the relation of these subtle transient warming events to the variability recorded in the deep ocean is difficult to constrain, these events are noteworthy as they exceed the (regional) variability observed in most of the Paleocene (Fig. 2). Although these events can only be revealed in high-resolution data generated for background climates, such data is currently scarce. Yet, resolving such signals from background noise, could prove essential to understand (Paleogene) climate and carbon cycle behavior (Sluijs et al., 2007; Bowen et al., 2015; Armstrong McKay and Lenton, 2018).

Potential for brGMGT proxies

Collectively, we find that the strong correlations with other reconstructed environmental parameters including MAAT and SST support a temperature-related response in brGMGTs. However, their common presence in lakes, peats and marine sediments implies that it is challenging to accurately assign observed variability to either air or sea surface temperature, or other parameters indirectly related to temperature (Kirkels et al., 2022). Despite this, we note that both HMBT and brGMGTI follow MBT'$_{5Me}$-based MAAT trends and brGMGTI produces similar absolute MAAT estimates despite the lack of an environment-specific calibration.

Intriguingly, the HMBT not only corresponds in trend with MBT'$_{5Me}$-MAAT, but the ratios between the compounds (brGMGTs 1020 / 1020 + 1034 + 1048) are also virtually identical with the traditional MBT(acyclic; defined as brGDGT-Ia / brGDGT-Ia + IIa + IIIa including their 6-methyl counterparts (Weijers et al., 2007)), supporting the notion that these compounds have a shared origin and/or mechanistic purpose in microbial membranes. In addition, the increase in brGMGT abundance relative to that of regular brGDGTs (%brGMGT) across the onset of the CIE may imply that the formation of H-shaped compounds represents an additional temperature adaptation (Morii et al., 1998; Naafs et al., 2018a) and/or that production of brGMGTs increased relative to that of brGDGTs in specific (i.e. marine) source areas (Kirkels et al., 2022). Despite these unknowns, the clear correlation to reconstructed environmental parameters and the ubiquitous presence of brGMGTs in these (shallow) marine settings such as sampled at Point Margaret highlight the potential for new paleoenvironment proxies based on brGMGTs once their origin and function are better resolved.

No temperature differences between the Australo-Antarctic Gulf and the Southwest Pacific?

We find identical absolute temperatures, both marine and terrestrial, within proxies and temperature trends in the AAG and the SW Pacific for all analyzed intervals (i.e., late Paleocene, PETM and EECO; Fig. 4). This could be assumed consistent with the similar paleolatitudes of the investigated sites (60–65ºS). However, it is difficult to reconcile with the proposed large-scale ocean circulation patterns, i.e., the warm low-latitude PLC in the AAG and cooler higher-latitude TC in the SW Pacific, across the analyzed interval (Fig. 1). It also contrasts with modeled differences in SST and MAAT between the areas east and west of the Tasman Gateway.

It is remarkable that not only the trends (Fig. 3), but also the reconstructed absolute TEX_{86}-based temperatures are similar across analyzed sections in the marine

realm (Fig. 4). While a seasonality bias in SST proxies could affect latitudinal gradients through dominance of warm-season productivity at higher latitudes (e.g. Antoine et al., 1996), it is unlikely that such effects would eliminate zonal differences (Fig. 4). Modern examples, such as the SST difference between the eastern and western North Atlantic that can exceed 5º C (e.g. Gouretski and Koltermann, 2004), support the notion that substantial zonal differences, such as those expected across the Tasman Gateway, should be detectable in proxy data.

One aspect that warrants exploration is the contribution of deep-water derived isoGDGTs and their potential impact on TEX_{86}-derived temperature reconstructions. While isoGDGT-producing Thaumarcheota occur through the entire water column, their highest concentrations are generally found near the lower part of the mixed layer, in the nitrite maximum, around 50–150m depth (e.g. Pitcher et al., 2011; Hurley et al., 2016; Hurley et al., 2018). The contribution of deep-water derived isoGDGTs can be assessed using [2/3] (e.g. Taylor et al., 2013; Kim et al., 2015; Hurley et al., 2018), which is based on the observation that [2/3] in suspended particulate matter (SPM) increases rapidly below 150-200m depth ([2/3] of ~3 up to ~200m depth, ~25 at >200m depth) (e.g. Hernández-Sánchez et al., 2014; Hurley et al., 2018). Low [2/3] are observed for the TEX_{86} datasets used here: Point Margaret (average 2), ODP1172 (2.5–3.5 for Paleocene-Eocene, 2.6 for EECO), Mid-Waipara (2.5), Hampden Beach (1.6) and U1356A (1.6), which, at face value, suggests contribution of deep-water derived isoGDGTs were minor. We therefore find [2/3] differences between the localities used here do not reveal any obvious differences in isoGDGT production depths.

The reconstructed temperatures and trends for the AAG relative to those in the SW Pacific increase the geographical extent of the discrepancy between modeled and proxy-derived temperatures in the high southern latitudes (Hollis et al., 2012; Lunt et al., 2021). At the same time, the findings for the AAG imply that the model-data discrepancy is not limited to the SW Pacific, but extends into the AAG (Lunt et al., 2021). Moreover, this zonal pattern did not notably change during intervals of both transient (PETM) and multi-million-year global warming (Late Paleocene-EECO). The temperature patterns exist within the marine and terrestrial realms and are evident in fundamentally different proxies for both realms. This seems to reinforce the existence of anomalously high SSTs in the AAG and particular the SW Pacific and it appears unlikely that the discrepancy can be resolved by an improved mechanistic understanding of a single SST proxy. While the MAAT for both regions, as for SST proxies, is indistinguishable, the absolute reconstructed MAATs are often *ca.* 10 ºC below SST (see also e.g. Bijl et al., 2021) and in relatively close agreement with modeled MAAT at high pCO_2 (e.g. Lunt et al., 2021; Reichgelt et al., 2022).

It remains uncertain how accurate the reconstructed absolute mean annual temperatures from the individual proxies are. For example, culture experiments emulating the non-analogue high-latitude conditions, such as the seasonal contrasts in light conditions in combination with high-temperature, are yet lacking. Constraining proxy behavior under climate conditions such as those that prevailed in the high southern latitudes during the early Paleogene might prove crucial to assess the value of currently available and forthcoming data. In the following section, we explore and revisit new and previously proposed options that may merit further attention in order to improve our understanding of deep-time high-latitude climate.

Spatial biases in the proxy and modeled temperature signals

In general, the inherent heterogeneity of hinterlands and, by extension, sourcing and transport of terrestrial components, particularly pollen and spores, gives rise to several challenges and may complicate a robust comparison between localities (e.g. Inglis et al., 2019). Challenges include changes in the catchment area, including vegetation source, river flow path, coastal proximity, altitude, and spatial integration. While this may affect some interpretations that rely on whole assemblages or presence/absence data (NLR), we suggest that this is likely a relatively minor issue for lowland or coastal taxa and indeed much of the study area. We find this assumption is warranted by the apparently synchronous appearance of *Nypa* across the TG, the relatively short time span of the studied time interval, and the fact that all records come from passive margins, implying that major tectonic changes in the catchment area are unlikely. However, comparing to localities further offshore or regions with strong (paleo)relief will invariably include some of these factors.

As the above factors mostly affect terrestrial proxy data, it is unlikely that invoking one single effect (e.g., seasonal biases, sourcing) resolves much of the model-data discrepancy. However, until recently, one effect on marine temperature proxies may have been largely overlooked. There is a dominance of records from near-shore, shallow and coastal environments in the compilation, an inherent (preservation) bias of many deep-time temperature reconstructions. Modern marginal marine settings generally experience greater influence of nearby landmasses and, partly as a consequence, more pronounced seasonal SST variations (~10 ºC) compared to open marine or oceanic (typically <5 ºC) (Hirahara et al., 2014; Judd et al., 2020), and it is reasonable to assume this was similar in the Paleogene. A greater mean annual temperature range potentially exacerbates any seasonal bias that may exist in proxy data for example by further amplifying warm-season dominated proxy signals.

Lastly, the low-resolution (1º and greater) models the (paleo)climate modeling community relies on tend to strongly over- or underestimate temperature in specific regions due to lack of fine-scale oceanographic features such as meso-scale eddies. The effects of this are most pronounced in regions associated with eastern and western boundary currents (Judd et al., 2020). Comparing the, mostly near-shore, paleoclimate reconstructions to low horizontal resolution model simulations may be complicated by such effects (Judd et al., 2020; Nooteboom et al., 2021), especially for regions with complex (paleo)geography. As these factors are challenging to constrain, and impact is likely to be site-specific it is difficult to gauge whether and how this may influence our ability to constrain and compare regional temperature patterns.

Influence of paleogeography

On a global scale and over latitudinally averaged zones, climate models can now reproduce proxy data (Cramwinckel et al., 2018; Evans et al., 2018), but an accurate representation of the global, local and regional paleogeography becomes important for finer scale model-data comparisons (Lunt et al., 2016; Frieling et al., 2017; Nooteboom et al., 2020; Nooteboom et al., 2021). The paleogeography of the region around the Tasman Gateway includes many continental blocks of uncertain paleobathymetry (Williams et al., 2019), which means that even if fully coupled simulations were to be run in higher spatial resolution, uncertainty in paleobathymetry/paleogeography may still impact temperature distribution. However, extreme end-member early Paleogene (prior to *ca.* 50 Ma) TG geographies with either deep throughflow or high topography have predictable climatic and oceanographic consequences (Bijl et al., 2011; Sijp et al., 2011; Sijp et al., 2016; Sauermilch et al.,

685 2021) that remain unsupported by the combination of tectonic, biogeographic and
686 temperature proxy data (Baatsen et al., 2018). This implies that such drastic changes
687 in paleogeographic boundary conditions are not primary candidates to resolve the
688 regional discrepancy between data and models.
689 Although the paleobathymetry of the SW Pacific itself has received less
690 attention than Southern Ocean gateways (Lagabrielle et al., 2009; Bijl et al., 2013a;
691 van de Lagemaat et al., 2021), recent work has suggested that sectors of the now
692 submerged continental plates of Zealandia may have been shallow or even emerged
693 above sea level during the Paleogene (Sutherland et al., 2019). The exact influence of
694 bathymetric features on the surface and deep ocean flow and heat distribution in this
695 region is yet unknown, but likely important for the exact configuration and shape of
696 the South Pacific polar gyre and thereby the direction of the proto-East-Australian
697 Current, as has been argued for other regions of deep-water formation (Coxall et al.,
698 2018; Vahlenkamp et al., 2018).
699 Apart from regional or local details in paleogeography, the use of either a
700 hotspot or paleo-magnetic reference frame for absolute paleolatitude reconstructions
701 may have a large impact on modeled oceanography at the sites used in this study. The
702 type of framework does not notably affect the positions of the sites relative to each
703 other, but the paleomagnetic framework shifts localities around the TG ca. 5 (±5)º
704 latitude north (Seton et al., 2012; van Hinsbergen et al., 2015; Müller et al., 2019), so
705 relative to the spin axis of the Earth. While this may seem trivial, much of the region
706 is within a latitudinal band that is highly sensitive to such changes (Baatsen et al.,
707 2020). Specifically, placing the same regional geography at lower latitudes implies
708 that there is a higher probability of wind-driven surface currents entering the
709 Australo-Antarctic Gulf and the SW Pacific through the Proto-Leeuwin current (PLC)
710 and Proto East-Australia current (PEAC), respectively, an effect that is independent of
711 model resolution (Baatsen et al., 2018; Nooteboom et al., 2021). Ultimately, the
712 minor shifts in paleolatitude may therefore have major impact on the origin and
713 temperature of water masses bathing sites east of the TG.
714
715 *Low-latitude current invasion into the SW Pacific and Australo-Antarctic Gulf*
716 Intriguingly, recent high-resolution (0.1º) ocean model simulations show an invasive
717 PEAC in the middle Eocene, penetrating as far south as ~55º S (Nooteboom et al.,
718 2021), bringing it within reach of some SW Pacific sites (e.g. DSDP 277, New
719 Zealand) unlike previous simulations (e.g., Huber et al., 2004; Hollis et al., 2012). A
720 shallow connection between the AAG and the SW Pacific may have existed in the
721 early Paleogene and would be in line with a superficial similarity of the dinocyst
722 assemblages from ODP Site 1172 and Point Margaret and Latrobe-1. However,
723 dinocyst bioprovinces are generally not well-defined in the Paleocene and earliest
724 Eocene, with the majority of taxa likely having a cosmopolitan distribution (e.g.
725 Frieling and Sluijs, 2018), implying similarity on either side did not necessitate an
726 open Tasman Gateway and associated warm or cold through flow.
727 While the observed biogeographic separation in the Middle and Late Eocene
728 (Huber et al., 2004; Bijl et al., 2011; Cramwinckel et al., 2020) may be interpreted as
729 the expression of a temperature or oceanographic difference, most modern and extinct
730 dinocysts, including thermophilic taxa such as *Apectodinium* have a wide temperature
731 tolerance (Prebble et al., 2013; Zonneveld et al., 2013; Frieling and Sluijs, 2018).
732 Therefore, it is much more likely that a combination of local environmental
733 parameters, including, for example, nutrient availability, coastal proximity and
734 salinity (Bijl et al., 2021), ultimately determined the assemblage characteristics and

735 therefore regional biogeography (Bijl et al., 2011; Zonneveld et al., 2013). In this
736 sense, previous interpretations of corresponding modeled high or low SST and
737 biogeography may have overstated the influence of SST on dinocyst biogeography.
738 With the currently available evidence from emergent high-resolution (0.1º)
739 ocean model runs we consider "warm"-current invasion into the SW Pacific and AAG
740 as the leading mechanism for forcing similar temperatures east and west of the
741 Tasman Gateway. This however does not yet explain the extremely high temperatures
742 in the high-latitude AAG or SW Pacific. Particularly temperatures from SST proxies
743 remain difficult to obtain from models that for other regions and MAAT proxies
744 produce similar results.
745
746 **Conclusions**
747 The southwest Pacific Ocean (~50–60ºS paleolatitude) was anomalously warm
748 through much of the early Paleogene, and proxy SSTs exceed modeled SST by ~10
749 ºC. Our data extend the area with extremely high proxy temperatures westward into
750 the AAG, with broad implications for reconstruction of meridional temperature
751 gradients and polar amplification that would be based on zonally averaged
752 temperature or temperature patterns and general ocean circulation.
753 The new multi-proxy temperature records from the AAG reveal a long-term
754 Late Paleocene warming on land and in the ocean, and, superimposed, two Late
755 Paleocene transient 'precursor' warming events, some ~300–400 and ~100 kyr prior
756 to the PETM. The origin, geographical extent and magnitude of these transient events
757 remain uncertain, but the existence of such relatively pronounced (regional)
758 variability is remarkable.
759 The new data also emphasizes the persistence of high, but similar absolute
760 temperatures and temperature evolution on both sides of a likely closed Tasman
761 Gateway through the warmest periods of the Paleogene (late Paleocene, PETM and
762 EECO). A strong influence of low-latitude ocean currents on both sides of the
763 Tasman Gateway is not expected based on marine microfossil distributions or low-
764 resolution models, yet should not be discarded as a mechanism that contributed to
765 excessive regional warmth and particularly similar temperatures east and west of the
766 TG.
767 A scenario with (seasonal) low-latitude influences on both sides of the Tasman
768 Gateway may become a preferred scenario when high-resolution (eddy-resolving)
769 modeling can be shown to accurately represent surface water conditions in the
770 Paleocene-Eocene Southern Ocean. Moreover, the difference between low and high-
771 resolution climate model runs may shed some light on SST over- or underestimates
772 east and west of the Tasman Gateway. In addition, a more accurate representation of
773 seasonality in the coastal-marginal marine settings may aid in resolving the influence
774 of proxy biases.
775 However, even if part of the model-data discrepancy can be resolved by higher-
776 resolution climate modeling, including an accurate representation of paleogeography,
777 it is likely other challenges, such as the offset between SST and MAAT estimates,
778 still limit our understanding of these distinctly non-analogue climates as they
779 prevailed in the southern mid to high-latitudes. Some of these directly complicate
780 comparison of proxy data to climate models, such as the influence of paleogeographic
781 and paleobathymetric boundary conditions; factors that are both difficult to
782 reconstruct and to accurately represent in models.
783
784 **Acknowledgments**

We thank G. Dammers, E.P. Huurdeman, K. Nierop, C. Rem and A. van Leeuwen for assistance in palynological processing and organic geochemical analyses. E. Hopmans is thanked for assistance and discussions on UHPLC-MS data. E.P. Huurdeman is acknowledged for work on the Latrobe-1 core as part of a Master's thesis. SJG was supported by the Australian IODP office. JP acknowledges support by the German Research Foundation (DFG; grant PR 651/24-1). AS thanks the European Research Council for consolidator grant #771497. PKB acknowledges support from NWO Vernieuwingsimpuls Veni grant no 863.13.002.

Data availability

All newly generated data has been submitted and will be available via the Pangaea database upon publication (DOI to be added).

References

Antoine, D., Andrt, J.M., and Morel, A., 1996, Oceanic primary production: 2. Estimation at global scale from satellite (Coastal Zone Color Scanner) chlorophyll: Global Biogeochemical Cycles, v. 10, no. 1, p. 57–69, doi: 10.1029/95GB02832.

Armstrong McKay, D.I., and Lenton, T.M., 2018, Reduced carbon cycle resilience across the Palaeocene–Eocene Thermal Maximum: Climate of the Past, v. 14, no. 10, p. 1515–1527, doi: 10.5194/cp-14-1515-2018.

Baatsen, M., von der Heydt, A.S., Huber, M., Kliphuis, M.A., Bijl, P.K., Sluijs, A., and Dijkstra, H.A., 2018, Equilibrium state and sensitivity of the simulated middle-to-late Eocene climate: Climate of the Past Discussions, , no. April, p. 1–49, doi: 10.5194/cp-2018-43.

Baatsen, M., Von Der Heydt, A.S., Huber, M., Kliphuis, M.A., Bijl, P.K., Sluijs, A., and Dijkstra, H.A., 2020, The middle to late Eocene greenhouse climate modelled using the CESM 1.0.5: Climate of the Past, v. 16, no. 6, p. 2573–2597, doi: 10.5194/cp-16-2573-2020.

Babila, T.L., Penman, D.E., Standish, C.D., Doubrawa, M., Bralower, T.J., Robinson, M.M., Self-trail, J.M., Speijer, R.P., Stassen, P., Foster, G.L., and Zachos, J.C., 2022, Surface ocean warming and acidification driven by rapid carbon release precedes Paleocene-Eocene Thermal Maximum: v. 1025, no. March, p. 1–14.

Bale, N.J., Palatinszky, M., Rijpstra, W.I.C., Herbold, C.W., Wagner, M., and Damsté, J.S.S., 2019, Membrane lipid composition of the moderately thermophilic ammonia-oxidizing archaeon "Candidatus Nitrosotenuis uzonensis" at different growth temperatures: Applied and Environmental Microbiology, v. 85, no. 20, doi: 10.1128/AEM.01332-19.

Baxter, A.J., van Bree, L.G.J., Peterse, F., Hopmans, E.C., Villanueva, L., Verschuren, D., and Sinninghe Damsté, J.S., 2021, Seasonal and multi-annual variation in the abundance of isoprenoid GDGT membrane lipids and their producers in the water column of a meromictic equatorial crater lake (Lake Chala, East Africa): Quaternary Science Reviews, v. 273, doi: 10.1016/j.quascirev.2021.107263.

Baxter, A.J., Hopmans, E.C., Russell, J.M., Sinninghe, J.S., Sinninghe Damsté, J.S., and Sinninghe, J.S., 2019, Bacterial GMGTs in East African lake sediments: Their potential as palaeotemperature indicators: Geochimica et Cosmochimica Acta, doi: 10.1016/j.gca.2019.05.039.

Bijl, P.K., Bendle, J.A.P., Bohaty, S.M., Pross, J., Schouten, S., Tauxe, L., Stickley, C.E., McKay, R.M., Rohl, U., Olney, M., Sluijs, A., Escutia, C., Brinkhuis, H., Klaus, A., et al., 2013a, Eocene cooling linked to early flow across the Tasmanian Gateway: Proceedings of the National Academy of Sciences, v. 110, no. 24, p. 9645–9650, doi: 10.1073/pnas.1220872110.

Bijl, P.K., Brinkhuis, H., Egger, L.M., Eldrett, J.S., Frieling, J., Grothe, A., Houben, A.J.P., Pross, J., Śliwińska, K.K., and Sluijs, A., 2016, Comment on ' Wetzeliella and its allies – the "hole" story: a taxonomic revision of the Paleogene dinoflagellate subfamily Wetzelielloideae' by Williams et al. (2015): Palynology, v. 6122, no. January 2017, p. 1–7, doi: 10.1080/01916122.2016.1235056.

Bijl, P.K., Frieling, J., Cramwinckel, M.J., Boschman, C., Sluijs, A., and Peterse, F., 2021, Maastrichtian-Rupelian paleoclimates in the southwest Pacific – a critical evaluation of biomarker paleothermometry and dinoflagellate cyst paleoecology at Ocean Drilling Program Site 1172: Climate of the Past, , no. March, p. 6, doi: 10.5194/cp-2021-18.

Bijl, P.K., Pross, J., Warnaar, J., Stickley, C.E., Huber, M., Guerstein, R., Houben, A.J.P., Sluijs, A., Visscher, H., and Brinkhuis, H., 2011, Environmental forcings of Paleogene Southern Ocean dinoflagellate biogeography: Paleoceanography, v. 26, no. 1, p. 1–12, doi: 10.1029/2009PA001905.

Bijl, P.K., Schouten, S., Sluijs, A., Reichart, G.-J., Zachos, J.C., and Brinkhuis, H., 2009, Early Palaeogene temperature evolution of the southwest Pacific Ocean: Nature, v. 461, no. 7265, p. 776–779, doi: 10.1038/nature08399.

Bijl, P.K., Sluijs, A., and Brinkhuis, H., 2013b, A magneto- and chemostratigraphically calibrated dinoflagellate cyst zonation of the early Palaeogene South Pacific Ocean: Earth-Science Reviews, v. 124, no. 0, p. 1–31, doi: http://dx.doi.org/10.1016/j.earscirev.2013.04.010.

Bowen, G.J., Maibauer, B.J., Kraus, M.J., Röhl, U., Westerhold, T., Steimke, A., Gingerich, P.D., Wing, S.L., and Clyde, W.C., 2015, Two massive, rapid releases of carbon during the onset of the Palaeocene-Eocene thermal maximum: Nature Geoscience, v. 8, no. 1, p. 44–47.

Burke, K.D., Williams, J.W., Chandler, M.A., Haywood, A.M., Lunt, D.J., and Otto-Bliesner, B.L., 2018, Pliocene and Eocene provide best analogs for near-future climates: Proceedings of the National Academy of Sciences, p. 201809600, doi: 10.1073/pnas.1809600115.

Cande, S.C., and Stock, J.M., 2004, Cenozoic reconstructions of the Australia-New Zealand-South Pacific sector of Antarctica, *in* Geophysical monograph series, p. 5–17.

Carpenter, R.J., Jordan, G.J., Macphail, M.K., and Hill, R.S., 2012, Near-tropical early eocene terrestrial temperatures at the Australo-Antarctic margin, western Tasmania: Geology, v. 40, no. 3, p. 267–270, doi: 10.1130/G32584.1.

Contreras, L., Pross, J., Bijl, P.K., Koutsodendris, A., Raine, J.I., van de Schootbrugge, B., and Brinkhuis, H., 2013, Early to Middle Eocene vegetation dynamics at the Wilkes Land Margin (Antarctica): Review of Palaeobotany and Palynology, v. 197, p. 119–142, doi: 10.1016/j.revpalbo.2013.05.009.

Contreras, L., Pross, J., Bijl, P.K., O'Hara, R.B., Raine, J.I., Sluijs, A., and Brinkhuis, H., 2014, Southern high-latitude terrestrial climate change during the Palaeocene–Eocene derived from a marine pollen record (ODP Site 1172, East Tasman Plateau): Climate of the Past, v. 10, no. 4, p. 1401–1420.

Coxall, H.K., Huck, C.E., Huber, M., Lear, C.H., Legarda-Lisarri, A., O'Regan, M., Sliwinska, K.K., Van De Flierdt, T., De Boer, A.M., Zachos, J.C., and Backman, J., 2018, Export of nutrient rich Northern Component Water preceded early Oligocene Antarctic glaciation /704/106/413 /704/829 /704/106/2738 article: Nature Geoscience, v. 11, no. 3, p. 190–196, doi: 10.1038/s41561-018-0069-9.

Cramer, B.S., Wright, J.D., Kent, D. V., and Aubry, M.-P., 2003, Orbital climate forcing of d13C excursions in the late Paleocene-early Eocene (chrons C24n-C25n): Paleoceanography, v. 18, no. 4, p. 21.

Cramwinckel, M.J., Huber, M., Kocken, I.J., Agnini, C., Bijl, P.K., Bohaty, S.M., Frieling, J., Goldner, A., Hilgen, F.J., Kip, E.L., Peterse, F., van der Ploeg, R., Röhl, U., Schouten, S., et al., 2018, Synchronous tropical and polar temperature evolution in the Eocene: Nature, v. 559, no. 7714, p. 382–386, doi: 10.1038/s41586-018-0272-2.

Cramwinckel, M.J., Woelders, L., Huurdeman, E.P., Peterse, F., Gallagher, S.J., Pross, J., Burgess, C.E., Reichart, G.J., Sluijs, A., and Bijl, P.K., 2020, Surface-circulation change in the southwest Pacific Ocean across the Middle Eocene Climatic Optimum: Inferences from dinoflagellate cysts and biomarker paleothermometry: Climate of the Past, v. 16, no. 5, p. 1667–1689, doi: 10.5194/cp-16-1667-2020.

Crouch, E.M., Willumsen, P.S., Kulhanek, D.K., and Gibbs, S.J., 2014, A revised Paleocene (Teurian) dinoflagellate cyst zonation from eastern New Zealand: Review of Palaeobotany and Palynology, v. 202, p. 47–79, doi: 10.1016/j.revpalbo.2013.12.004.

Dickens, G.R., O'Neil, J.R., Rea, D.K., and Owen, R.M., 1995, Dissociation of oceanic methane hydrate as a cause of the carbon isotope excursion at the end of the Paleocene: Paleoceanography, v. 10, no. 6, p. 965–971, doi: 10.1029/95PA02087.

Douglas, P.M.J., Affek, H.P., Ivany, L.C., Houben, A.J.P., Sijp, W.P., Sluijs, A., Schouten, S., and Pagani, M., 2014, Pronounced zonal heterogeneity in Eocene southern high-latitude sea surface temperatures.: Proceedings of the National Academy of Sciences of the United States of America, v. 111, no. 18, p. 1–6, doi: 10.1073/pnas.1321441111.

Dunkley Jones, T., Lunt, D.J., Schmidt, D.N., Ridgwell, A.J., Sluijs, A., Valdes, P.J., and Maslin, M.A., 2013, Climate model and proxy data constraints on ocean warming across the Paleocene–Eocene Thermal Maximum: Earth-Science Reviews, v. 125, no. 0, p. 123–145, doi: http://dx.doi.org/10.1016/j.earscirev.2013.07.004.

Evans, D., Sagoo, N., Renema, W., Cotton, L.J., Müller, W., Todd, J.A., Saraswati, P.K., Stassen, P., Ziegler, M., Pearson, P.N., Valdes, P.J., and Affek, H.P., 2018, Eocene greenhouse climate revealed by coupled clumped isotope-Mg/Ca thermometry: Proceedings of the National Academy of Sciences, v. 115, no. 6, p. 1174–1179, doi: 10.1073/pnas.1714744115.

Frieling, J., Gebhardt, H., Huber, M., Adekeye, O.A., Akande, S.O., Reichart, G.-J., Middelburg, J.J., Schouten, S., and Sluijs, A., 2017, Extreme warmth and heat-stressed plankton in the tropics during the Paleocene-Eocene Thermal Maximum: Science Advances, v. 3, no. 3, p. e1600891, doi: 10.1126/sciadv.1600891.

Frieling, J., Huurdeman, E.P., Rem, C.C.M., Donders, T.H., Pross, J., Bohaty, S.M., Holdgate, G.R., Gallagher, S.J., McGowran, B., and Bijl, P.K., 2018, Identification of the Paleocene–Eocene boundary in coastal strata in the Otway Basin, Victoria, Australia: Journal of Micropalaeontology, v. 37, no. 1, p. 317–339, doi: 10.5194/jm-37-317-2018.

Frieling, J., Peterse, F., Lunt, D.J.J., Bohaty, S.M.M., Damsté, J.S.S., Reichart, G. -J. -J., Sluijs, A., Sinninghe Damsté, J.S., Reichart, G. -J. -J., and Sluijs, A., 2019, Widespread Warming Before and Elevated Barium Burial During the Paleocene-Eocene Thermal Maximum: Evidence for Methane Hydrate Release? Paleoceanography and Paleoclimatology, p. 2018PA003425, doi: 10.1029/2018PA003425.

Frieling, J., and Sluijs, A., 2018, Towards quantitative environmental reconstructions from ancient

non-analogue microfossil assemblages: Ecological preferences of Paleocene – Eocene dinoflagellates: Earth-Science Reviews, v. 185, no. August, p. 956–973, doi: 10.1016/j.earscirev.2018.08.014.

Gouretski, V.V., and Koltermann, K.P., 2004, WOCE Global Hydrographic Climatology: Berichte des Bundesamtes fur Seeschifffahrt und Hydrographie, doi: 10.5065/GS51-V170.

Greenwood, D.R., Moss, P.T., Rowett, A.I., Vadala, A.J., and Keefe, R.L., 2003, Plant communities and climate change in southeastern Australia during the early Paleogene, *in* Special Paper 369: Causes and consequences of globally warm climates in the early Paleogene, Geological Society of America, p. 365–380.

Hernández-Sánchez, M.T., Woodward, E.M.S., Taylor, K.W.R., Henderson, G.M., and Pancost, R.D., 2014, Variations in GDGT distributions through the water column in the South East Atlantic Ocean: Geochimica et Cosmochimica Acta, v. 132, p. 337–348, doi: 10.1016/j.gca.2014.02.009.

Hines, B.R., Hollis, C.J., Atkins, C.B., Baker, J.A., Morgans, H.E.G., and Strong, P.C., 2017, Reduction of oceanic temperature gradients in the early Eocene Southwest Pacific Ocean: Palaeogeography, Palaeoclimatology, Palaeoecology, v. 475, p. 41–54, doi: 10.1016/j.palaeo.2017.02.037.

van Hinsbergen, D.J.J., de Groot, L. V, van Schaik, S.J., Spakman, W., Bijl, P.K., Sluijs, A., Langereis, C.G., and Brinkhuis, H., 2015, A Paleolatitude Calculator for Paleoclimate Studies: PloS one, v. 10, no. 6, p. e0126946, doi: 10.1371/journal.pone.0126946.

Hirahara, S., Ishii, M., and Fukuda, Y., 2014, Centennial-scale sea surface temperature analysis and its uncertainty: Journal of Climate, v. 27, no. 1, p. 57–75, doi: 10.1175/JCLI-D-12-00837.1.

Hollis, C.J., Dunkley Jones, T., Anagnostou, E., Bijl, P.K., Cramwinckel, M.J., Cui, Y., Dickens, G.R., Edgar, K.M., Eley, Y., Evans, D., Foster, G.L., Frieling, J., Inglis, G.N., Kennedy, E.M., et al., 2019, The DeepMIP contribution to PMIP4: methodologies for selection, compilation and analysis of latest Paleocene and early Eocene climate proxy data, incorporating version 0.1 of the DeepMIP database: Geoscientific Model Development, v. 12, no. 7, p. 3149–3206, doi: 10.5194/gmd-12-3149-2019.

Hollis, C.J., Handley, L., Crouch, E.M., Morgans, H.E.G., Baker, J.A., Creech, J., Collins, K.S., Gibbs, S.J., Huber, M., Schouten, S., Zachos, J.C., and Pancost, R.D., 2009, Tropical sea temperatures in the high-latitude South Pacific during the Eocene: Geology, v. 37, no. 2, p. 99–102, doi: 10.1130/G25200A.1.

Hollis, C.J., Hines, B.R., Littler, K., Villasante-Marcos, V., Kulhanek, D.K., Strong, C.P., Zachos, J.C., Eggins, S.M., Northcote, L., and Phillips, A., 2015, The Paleocene–Eocene Thermal Maximum at DSDP Site 277, Campbell Plateau, southern Pacific Ocean: Climate of the Past, v. 11, no. 7, p. 1009–1025, doi: 10.5194/cp-11-1009-2015.

Hollis, C.J., Taylor, K.W.R., Handley, L., Pancost, R.D., Huber, M., Creech, J.B., Hines, B.R., Crouch, E.M., Morgans, H.E.G., Crampton, J.S., Gibbs, S., Pearson, P.N., and Zachos, J.C., 2012, Early Paleogene temperature history of the Southwest Pacific Ocean: Reconciling proxies and models: Earth and Planetary Science Letters, v. 349–350, p. 53–66, doi: 10.1016/j.epsl.2012.06.024.

Hopmans, E.C., Weijers, J.W.H., Schefuß, E., Herfort, L., Sinninghe Damsté, J.S., and Schouten, S., 2004, A novel proxy for terrestrial organic matter in sediments based on branched and isoprenoid tetraether lipids: Earth and Planetary Science Letters, v. 224, no. 1–2, p. 107–116, doi: 10.1016/j.epsl.2004.05.012.

Huber, M., Brinkhuis, H., Stickley, C.E., Döös, K., Sluijs, A., Warnaar, J., Schellenberg, S.A., and Williams, G.L., 2004, Eocene circulation of the Southern Ocean: Was Antarctica kept warm by subtropical waters? Paleoceanography, v. 19, no. 4, p. n/a-n/a, doi: 10.1029/2004PA001014.

Huck, C.E., van de Flierdt, T., Bohaty, S.M., and Hammond, S.J., 2017, Antarctic climate, Southern Ocean circulation patterns, and deep water formation during the Eocene: Paleoceanography, v. 32, no. 7, p. 674–691, doi: 10.1002/2017PA003135.

Hurley, S.J., Elling, F.J., Könneke, M., Buchwald, C., Wankel, S.D., Santoro, A.E., Lipp, J.S., Hinrichs, K.-U., and Pearson, A., 2016, Influence of ammonia oxidation rate on thaumarchaeal lipid composition and the TEX86 temperature proxy: Proceedings of the National Academy of Sciences, v. 113, no. 28, p. 7762–7767, doi: 10.1073/pnas.1518534113.

Hurley, S.J., Lipp, J.S., Close, H.G., Hinrichs, K.U., and Pearson, A., 2018, Distribution and export of isoprenoid tetraether lipids in suspended particulate matter from the water column of the Western Atlantic Ocean: Organic Geochemistry, v. 116, p. 90–102, doi: 10.1016/j.orggeochem.2017.11.010.

Huurdeman, E.P., Frieling, J., Reichgelt, T., Bijl, P.K., Bohaty, S.M., Holdgate, G.R., Gallagher, S.J., Peterse, F., Greenwood, D.R., and Pross, J., 2021, Rapid expansion of meso-megathermal rain forests into the southern high latitudes at the onset of the Paleocene-Eocene Thermal Maximum:

Geology, doi: 10.1130/G47343.1.
Inglis, G.N., Farnsworth, A., Collinson, M.E., Carmichael, M.J., Naafs, B.D.A., Lunt, D.J., Valdes, P.J., Pancost, R.D., Matthew, J., Lunt, D.J., Valdes, P.J., Pancost, D., and Unit, O.G., 2019, Terrestrial environmental change across the onset of the PETM and the associated impact on biomarker proxies : a cautionary tale: Global and Planetary Change, v. 181, no. July, p. 102991, doi: 10.1016/j.gloplacha.2019.102991.
Inglis, G.N., Farnsworth, A., Lunt, D.J., Foster, G.L., Hollis, C.J., Pagani, M., Jardine, P.E., Pearson, P.N., Markwick, P.J., Galsworthy, A.M.J., Raynham, L., Taylor, K.W.R., and Pancost, R.D., 2015, Descent towards the Icehouse: Eocene sea surface cooling inferred from GDGT distributions: Paleoceanography, v. 30, no. 7, p. 1000–1020, doi: 10.1002/2014PA002723.
John, C.M., Banerjee, N.R., Longstaffe, F.J., Sica, C., Law, K.R., and Zachos, J.C., 2012, Clay assemblage and oxygen isotopic constraints on the weathering response to the Paleocene-Eocene thermal maximum, East Coast of North America: Geology, v. 40, no. 7, p. 591–594, doi: 10.1130/G32785.1.
De Jonge, C., Hopmans, E.C., Zell, C.I., Kim, J.-H., Schouten, S., and Sinninghe Damsté, J.S., 2014, Occurrence and abundance of 6-methyl branched glycerol dialkyl glycerol tetraethers in soils: Implications for palaeoclimate reconstruction: Geochimica et Cosmochimica Acta, v. 141, p. 97–112, doi: 10.1016/j.gca.2014.06.013.
Judd, E.J., Bhattacharya, T., and Ivany, L.C., 2020, A Dynamical Framework for Interpreting Ancient Sea Surface Temperatures: Geophysical Research Letters, v. 47, no. 15, doi: 10.1029/2020GL089044.
Kim, J.H., van der Meer, J., Schouten, S., Helmke, P., Willmott, V., Sangiorgi, F., Koç, N., Hopmans, E.C., and Damsté, J.S.S., 2010, New indices and calibrations derived from the distribution of crenarchaeal isoprenoid tetraether lipids: Implications for past sea surface temperature reconstructions: Geochimica et Cosmochimica Acta, v. 74, no. 16, p. 4639–4654, doi: 10.1016/j.gca.2010.05.027.
Kim, J.H., Schouten, S., Rodrigo-Gámiz, M., Rampen, S., Marino, G., Huguet, C., Helmke, P., Buscail, R., Hopmans, E.C., Pross, J., Sangiorgi, F., Middelburg, J.B.M., and Sinninghe Damsté, J.S., 2015, Influence of deep-water derived isoprenoid tetraether lipids on the TEX86H paleothermometer in the Mediterranean Sea: Geochimica et Cosmochimica Acta, v. 150, p. 125–141, doi: 10.1016/j.gca.2014.11.017.
Kirkels, F.M.S.A., Usman, M.O., and Peterse, F., 2022, Distinct sources of bacterial branched GMGTs in the Godavari River basin (India) and Bay of Bengal sediments: Organic Geochemistry, v. 167, no. February, p. 104405, doi: 10.1016/j.orggeochem.2022.104405.
De La Torre, J.R., Walker, C.B., Ingalls, A.E., Könneke, M., and Stahl, D.A., 2008, Cultivation of a thermophilic ammonia oxidizing archaeon synthesizing crenarchaeol: Environmental Microbiology, v. 10, no. 3, p. 810–818, doi: 10.1111/j.1462-2920.2007.01506.x.
Lagabrielle, Y., Goddéris, Y., Donnadieu, Y., Malavieille, J., and Suarez, M., 2009, The tectonic history of Drake Passage and its possible impacts on global climate: Earth and Planetary Science Letters, v. 279, no. 3–4, p. 197–211, doi: 10.1016/j.epsl.2008.12.037.
van de Lagemaat, S.H.A., Swart, M.L.A., Vaes, B., Kosters, M.E., Boschman, L.M., Burton-Johnson, A., Bijl, P.K., Spakman, W., and van Hinsbergen, D.J.J., 2021, Subduction initiation in the Scotia Sea region and opening of the Drake Passage: When and why? Earth-Science Reviews, p. 103551, doi: 10.1016/j.earscirev.2021.103551.
Lauretano, V., Littler, K., Polling, M., Zachos, J.C., and Lourens, L.J., 2015, Frequency, magnitude and character of hyperthermal events at the onset of the Early Eocene Climatic Optimum: Climate of the Past, v. 11, no. 10, p. 1313–1324, doi: 10.5194/cp-11-1313-2015.
Liu, X.L., Summons, R.E., and Hinrichs, K.U., 2012, Extending the known range of glycerol ether lipids in the environment: Structural assignments based on tandem mass spectral fragmentation patterns: Rapid Communications in Mass Spectrometry, v. 26, no. 19, p. 2295–2302, doi: 10.1002/rcm.6355.
Lunt, D.J., Bragg, F., Chan, W.-L., Hutchinson, D.K., Ladant, J.-B., Morozova, P., Niezgodzki, I., Steinig, S., Zhang, Z., Zhu, J., Abe-Ouchi, A., Anagnostou, E., de Boer, A.M., Coxall, H.K., et al., 2021, DeepMIP: model intercomparison of early Eocene climatic optimum (EECO) large-scale climate features and comparison with proxy data: Climate of the Past, v. 17, no. 1, p. 203–227, doi: 10.5194/cp-17-203-2021.
Lunt, D.J., Farnsworth, A., Loptson, C., L Foster, G., Markwick, P., O'Brien, C.L., Pancost, R.D., Robinson, S.A., and Wrobel, N., 2016, Palaeogeographic controls on climate and proxy interpretation: Climate of the Past, v. 12, no. 5, p. 1181–1198, doi: 10.5194/cp-12-1181-2016.
Lunt, D.J., Huber, M., Anagnostou, E., Baatsen, M.L.J., Caballero, R., DeConto, R., Dijkstra, H.A.,

Donnadieu, Y., Evans, D., Feng, R., Foster, G.L., Gasson, E., von der Heydt, A.S., Hollis, C.J., et al., 2017, The DeepMIP contribution to PMIP4: experimental design for model simulations of the EECO, PETM, and pre-PETM (version 1.0): Geoscientific Model Development, v. 10, no. 2, p. 889–901, doi: 10.5194/gmd-10-889-2017.

McInerney, F.A., and Wing, S.L., 2011, The Paleocene-Eocene thermal maximum: a perturbation of carbon cycle, climate, and biosphere with implications for the future: Annual Review of Earth and Planetary Sciences, v. 39, no. 1, p. 489–516, doi: 10.1146/annurev-earth-040610-133431.

Morii, H., Eguchi, T., Nishihara, M., Kakinuma, K., König, H., and Koga, Y., 1998, A novel ether core lipid with H-shaped C80-isoprenoid hydrocarbon chain from the hyperthermophilic methanogen Methanothermus fervidus: Biochimica et Biophysica Acta - Lipids and Lipid Metabolism, v. 1390, no. 3, p. 339–345, doi: 10.1016/S0005-2760(97)00183-5.

Müller, R.D., Zahirovic, S., Williams, S.E., Cannon, J., Seton, M., Bower, D.J., Tetley, M.G., Heine, C., Le Breton, E., Liu, S., Russell, S.H.J., Yang, T., Leonard, J., and Gurnis, M., 2019, A Global Plate Model Including Lithospheric Deformation Along Major Rifts and Orogens Since the Triassic: Tectonics, v. 38, no. 6, p. 1884–1907, doi: 10.1029/2018TC005462.

Naafs, B.D.A., Inglis, G.N., Zheng, Y., Amesbury, M.J., Biester, H., Bindler, R., Blewett, J., Burrows, M.A., del Castillo Torres, D., Chambers, F.M., Cohen, A.D., Evershed, R.P., Feakins, S.J., Gallego-Sala, A., et al., 2017, Introducing global peat-specific temperature and pH calibrations based on brGDGT bacterial lipids: Geochimica et Cosmochimica Acta, v. 208, no. June 2016, p. 285–301, doi: 10.1016/j.gca.2017.01.038.

Naafs, B.D.A., McCormick, D., Inglis, G.N., and Pancost, R.D., 2018a, Archaeal and bacterial H-GDGTs are abundant in peat and their relative abundance is positively correlated with temperature: Geochimica et Cosmochimica Acta, v. 227, p. 156–170, doi: 10.1016/j.gca.2018.02.025.

Naafs, B.D.A., Rohrssen, M., Inglis, G.N., Lähteenoja, O., Feakins, S.J., Collinson, M.E., Kennedy, E.M., Singh, P.K., Singh, M.P., Lunt, D.J., and Pancost, R.D., 2018b, High temperatures in the terrestrial mid-latitudes during the early Palaeogene: Nature Geoscience, v. 11, no. 10, p. 766–771, doi: 10.1038/s41561-018-0199-0.

Nooteboom, P.D., Baatsen, M., Bijl, P.K., Michael, A., Sebille, E. Van, Sluijs, A., and Dijkstra, H.A., 2021, Strongly eddying ocean simulations required to resolve Eocene model-data mismatch: , p. 1–23, doi: 10.1002/essoar.10508749.1.

Nooteboom, P.D., Delandmeter, P., van Sebille, E., Bijl, P.K., Dijkstra, H.A., and von der Heydt, A.S., 2020, Resolution dependency of sinking Lagrangian particles in ocean general circulation models: PLoS ONE, v. 15, no. 9 September, p. 1–16, doi: 10.1371/journal.pone.0238650.

O'Brien, C.L., Robinson, S.A., Pancost, R.D., Sinninghe Damsté, J.S., Schouten, S., Lunt, D.J., Alsenz, H., Bornemann, A., Bottini, C., Brassell, S.C., Farnsworth, A., Forster, A., Huber, B.T., Inglis, G.N., et al., 2017, Cretaceous sea-surface temperature evolution: Constraints from TEX 86 and planktonic foraminiferal oxygen isotopes: Earth-Science Reviews, v. 172, no. March 2016, p. 224–247, doi: 10.1016/j.earscirev.2017.07.012.

Pak, D.K., and Miller, K.G., 1992, Paleocene to Eocene benthic foraminiferal isotopes and assemblages: implications for deepwater circulation: Paleoceanography, v. 7, no. 4, p. 405–422.

Pancost, R.D., Taylor, K.W.R., Inglis, G.N., Kennedy, E.M., Handley, L., Hollis, C.J., Crouch, E.M., Pross, J., Huber, M., Schouten, S., Pearson, P.N., Morgans, H.E.G., and Raine, J.I., 2013, Early Paleogene evolution of terrestrial climate in the SW Pacific, Southern New Zealand: Geochemistry, Geophysics, Geosystems, v. 14, no. 12, p. 5413–5429, doi: 10.1002/2013GC004935.

Pitcher, A., Villanueva, L., Hopmans, E.C., Schouten, S., Reichart, G.J., and Sinninghe Damsté, J.S., 2011, Niche segregation of ammonia-oxidizing archaea and anammox bacteria in the Arabian Sea oxygen minimum zone: ISME Journal, v. 5, no. 12, p. 1896–1904, doi: 10.1038/ismej.2011.60.

Prebble, J.G., Crouch, E.M., Carter, L., Cortese, G., Bostock, H., and Neil, H., 2013, An expanded modern dinoflagellate cyst dataset for the Southwest Pacific and Southern Hemisphere with environmental associations: Marine Micropaleontology, v. 101, p. 33–48, doi: 10.1016/j.marmicro.2013.04.004.

Pross, J., Contreras, L., Bijl, P.K., Greenwood, D.R., Bohaty, S.M., Schouten, S., Bendle, J.A.P., Röhl, U., Tauxe, L., Raine, J.I., Huck, C.E., Van De Flierdt, T., Jamieson, S.S.R., Stickley, C.E., et al., 2012, Persistent near-tropical warmth on the Antarctic continent during the early Eocene epoch: Nature, v. 487, no. 7409, p. 73–77, doi: 10.1038/nature11300.

Reichgelt, T., Greenwood, D.R., Steinig, S., Conran, J.G., Hutchinson, D.K., Lunt, D.J., Scriven, L.J., and Zhu, J., 2022, Plant Proxy Evidence for High Rainfall and Productivity in the Eocene of

Australia:
Reichgelt, T., West, C.K., and Greenwood, D.R., 2018, The relation between global palm distribution and climate: Scientific Reports, v. 8, no. 1, p. 4721, doi: 10.1038/s41598-018-23147-2.
Sauermilch, I., Whittaker, J.M., Bijl, P.K., Totterdell, J.M., and Jokat, W., 2019, Tectonic, Oceanographic, and Climatic Controls on the Cretaceous-Cenozoic Sedimentary Record of the Australian-Antarctic Basin: Journal of Geophysical Research: Solid Earth, v. 124, no. 8, p. 7699–7724, doi: 10.1029/2018JB016683.
Sauermilch, I., Whittaker, J.M., Klocker, A., Munday, D.R., Hochmuth, K., Bijl, P.K., and LaCasce, J.H., 2021, Gateway-driven weakening of ocean gyres leads to Southern Ocean cooling: Nature Communications, v. 12, no. 1, p. 1–8, doi: 10.1038/s41467-021-26658-1.
Schneider-Mor, A., and Bowen, G.J., 2013, Coupled and decoupled responses of continental and marine organic-sedimentary systems through the Paleocene-Eocene thermal maximum, New Jersey margin, USA: Paleoceanography, v. 28, no. 1, p. 105–115, doi: 10.1002/palo.20016.
Schouten, S., Baas, M., Hopmans, E.C., Reysenbach, A.L., and Damsté, J.S.S., 2008, Tetraether membrane lipids of Candidatus "Aciduliprofundum boonei", a cultivated obligate thermoacidophilic euryarchaeote from deep-sea hydrothermal vents: Extremophiles, v. 12, no. 1, p. 119–124, doi: 10.1007/s00792-007-0111-0.
Schouten, S., Hopmans, E.C., Schefuß, E., and Sinninghe Damsté, J.S., 2002, Distributional variations in marine crenarchaeotal membrane lipids: a new tool for reconstructing ancient sea water temperatures? Earth and Planetary Science Letters, v. 204, no. 1–2, p. 265–274, doi: 10.1016/S0012-821X(02)00979-2.
Schouten, S., Hopmans, E.C., and Sinninghe Damsté, J.S., 2013, The organic geochemistry of glycerol dialkyl glycerol tetraether lipids: A review: Organic Geochemistry, v. 54, no. 0, p. 19–61, doi: 10.1016/j.orggeochem.2012.09.006.
Secord, R., Gingerich, P.D., Lohmann, K.C., and MacLeod, K.G., 2010, Continental warming preceding the Palaeocene-Eocene thermal maximum: Nature, v. 467, no. 7318, p. 955–958, doi: 10.1038/nature09441.
Seton, M., Müller, R.D., Zahirovic, S., Gaina, C., Torsvik, T.H., Shephard, G., Talsma, A., Gurnis, M., Turner, M., and Maus, S., 2012, Global continental and ocean basin reconstructions since 200Ma: Earth-Science Reviews, v. 113, no. 3, p. 212–270.
Sijp, W.P., England, M.H., and Huber, M., 2011, Effect of the deepening of the Tasman Gateway on the global ocean: Paleoceanography, v. 26, no. 4, p. 1–18, doi: 10.1029/2011PA002143.
Sijp, W.P., von der Heydt, A.S., and Bijl, P.K., 2016, Model simulations of early westward flow across the Tasman Gateway during the early Eocene: Climate of the Past, v. 12, no. 4, p. 807–817, doi: 10.5194/cp-12-807-2016.
Sijp, W.P., von der Heydt, A.S., Dijkstra, H.A., Flögel, S., Douglas, P.M.J.J., and Bijl, P.K., 2014, The role of ocean gateways on cooling climate on long time scales: Global and Planetary Change, v. 119, p. 1–22, doi: 10.1016/j.gloplacha.2014.04.004.
Sinninghe Damsté, J.S., Irene C. Rijpstra, W., Hopmans, E.C., den Uijl, M.J., Weijers, J.W.H., and Schouten, S., 2018, The enigmatic structure of the crenarchaeol isomer: Organic Geochemistry, doi: 10.1016/j.orggeochem.2018.06.005.
Sinninghe Damsté, J.S., Ossebaar, J., Schouten, S., and Verschuren, D., 2012, Distribution of tetraether lipids in the 25-ka sedimentary record of Lake Challa: Extracting reliable TEX 86 and MBT/CBT palaeotemperatures from an equatorial African lake: Quaternary Science Reviews, v. 50, p. 43–54, doi: 10.1016/j.quascirev.2012.07.001.
Sinninghe Damsté, J.S., Schouten, S., Hopmans, E.C., Van Duin, A.C.T., and Geenevasen, J.A.J., 2002, Crenarchaeol: The characteristic core glycerol dibiphytanyl glycerol tetraether membrane lipid of cosmopolitan pelagic crenarchaeota: Journal of Lipid Research, v. 43, no. 10, p. 1641–1651, doi: 10.1194/jlr.M200148-JLR200.
Sluijs, A., Bijl, P.K., Schouten, S., Röhl, U., Reichart, G.-J., and Brinkhuis, H., 2011, Southern ocean warming, sea level and hydrological change during the Paleocene-Eocene thermal maximum: Climate of the Past, v. 7, no. 1, p. 47–61, doi: 10.5194/cp-7-47-2011.
Sluijs, A., Brinkhuis, H., Schouten, S., Bohaty, S.M., John, C.M., Zachos, J.C., Reichart, G.-J., Sinninghe Damsté, J.S., Crouch, E.M., and Dickens, G.R., 2007, Environmental precursors to rapid light carbon injection at the Palaeocene/Eocene boundary.: Nature, v. 450, no. 7173, p. 1218–1221, doi: 10.1038/nature06400.
Sluijs, A., Frieling, J., Inglis, G.N., Nierop, K.G.J., Peterse, F., Sangiorgi, F., and Schouten, S., 2020, Late Paleocene–early Eocene Arctic Ocean sea surface temperatures: reassessing biomarker paleothermometry at Lomonosov Ridge: Climate of the Past, v. 16, no. 6, p. 2381–2400, doi: 10.5194/cp-16-2381-2020.

Sutherland, R., Dickens, G.R., Blum, P., Agnini, C., Alegret, L., Asatryan, G., Bhattacharya, J., Bordenave, A., Chang, L., Collot, J., Cramwinckel, M.J., Dallanave, E., Drake, M.K., Etienne, S.J.G., et al., 2019, Expedition 371 summary.

Taylor, K.W.R., Huber, M., Hollis, C.J., Hernandez-Sanchez, M.T., and Pancost, R.D., 2013, Re-evaluating modern and Palaeogene GDGT distributions: Implications for SST reconstructions: Global and Planetary Change, v. 108, p. 158–174, doi: 10.1016/j.gloplacha.2013.06.011.

Thomas, D.J., Zachos, J.C., Bralower, T.J., Thomas, E., and Bohaty, S.M., 2002, Warming the Fuel for the Fire : Evidence for the Thermal Dissociation of Methane Hydrate During the Paleocene-Eocene Thermal Maximum dissociation of methane hydrate during the Paleocene-Eocene: Geology, v. 30, no. 12, p. 1067–1070, doi: 10.1130/0091-7613(2002)030<1067:WTFFTF>2.0.CO;2.

Tierney, J.E., and Tingley, M.P., 2015, A TEX86 surface sediment database and extended Bayesian calibration: Scientific Data, v. 2, p. 150029, doi: 10.1038/sdata.2015.29.

Vahlenkamp, M., Niezgodzki, I., De Vleeschouwer, D., Lohmann, G., Bickert, T., and Pälike, H., 2018, Ocean and climate response to North Atlantic seaway changes at the onset of long-term Eocene cooling: Earth and Planetary Science Letters, v. 498, p. 185–195, doi: 10.1016/j.epsl.2018.06.031.

Weijers, J.W.H., Schouten, S., van den Donker, J.C., Hopmans, E.C., and Sinninghe Damsté, J.S., 2007, Environmental controls on bacterial tetraether membrane lipid distribution in soils: Geochimica et Cosmochimica Acta, v. 71, no. 3, p. 703–713, doi: 10.1016/j.gca.2006.10.003.

Weijers, J.W.H., Schouten, S., Spaargaren, O.C., and Sinninghe Damsté, J.S., 2006, Occurrence and distribution of tetraether membrane lipids in soils: Implications for the use of the TEX86 proxy and the BIT index: Organic Geochemistry, v. 37, no. 12, p. 1680–1693, doi: 10.1016/j.orggeochem.2006.07.018.

Westerhold, T., Marwan, N., Drury, A.J., Liebrand, D., Agnini, C., Anagnostou, E., Barnet, J.S.K., Bohaty, S.M., De Vleeschouwer, D., Florindo, F., Frederichs, T., Hodell, D.A., Holbourn, A.E., Kroon, D., et al., 2020, An astronomically dated record of Earth's climate and its predictability over the last 66 million years: Science, v. 369, no. 6509, p. 1383–1388, doi: 10.1126/SCIENCE.ABA6853.

Westerhold, T., Röhl, U., Donner, B., and Zachos, J.C., 2018, Global Extent of Early Eocene Hyperthermal Events: A New Pacific Benthic Foraminiferal Isotope Record From Shatsky Rise (ODP Site 1209): Paleoceanography and Paleoclimatology, v. 0, no. ja, p. 1–17, doi: 10.1029/2017PA003306.

Williams, G.L., Fensome, R.A., and MacRae, R.A., 2017, The Lentin and Williams index of fossil dinoflagellates 2017 edition.: American Association of Petroleum Geologists Contribution Series, v. 48.

Williams, S.E., Whittaker, J.M., Halpin, J.A., and Müller, R.D., 2019, Australian-Antarctic breakup and seafloor spreading: Balancing geological and geophysical constraints: Earth-Science Reviews, v. 188, no. September 2018, p. 41–58, doi: 10.1016/j.earscirev.2018.10.011.

Xie, S., Liu, X.-L., Schubotz, F., Wakeham, S.G., and Hinrichs, K.-U., 2014, Distribution of glycerol ether lipids in the oxygen minimum zone of the Eastern Tropical North Pacific Ocean: Organic Geochemistry, v. 71, p. 60–71, doi: 10.1016/j.orggeochem.2014.04.006.

Zachos, J.C., Rohl, U., Schellenberg, S.A., Sluijs, A., Hodell, D.A., Kelly, D.C., Thomas, E., Nicolo, M.J., Raffi, I., Lourens, L.J., McCarren, H.K., and Kroon, D., 2005, Rapid Acidification of the Ocean During the Paleocene-Eocene Thermal Maximum: Science, v. 308, no. 5728, p. 1611–1615, doi: 10.1126/science.1109004.

Zhang, Y.G., Pagani, M., and Wang, Z., 2016, Ring Index: A new strategy to evaluate the integrity of TEX 86 paleothermometry: Paleoceanography, v. 31, no. 2, p. 220–232, doi: 10.1002/2015PA002848.

Zhang, Y.G., Zhang, C.L., Liu, X.L., Li, L., Hinrichs, K.U., and Noakes, J.E., 2011, Methane Index: A tetraether archaeal lipid biomarker indicator for detecting the instability of marine gas hydrates: Earth and Planetary Science Letters, v. 307, no. 3–4, p. 525–534, doi: 10.1016/j.epsl.2011.05.031.

Zhu, J., Poulsen, C.J., and Tierney, J.E., 2019, Simulation of Eocene extreme warmth and high climate sensitivity through cloud feedbacks: Science Advances, v. 5, no. 9, p. eaax1874, doi: 10.1126/sciadv.aax1874.

Zonneveld, K.A.F., Marret, F., Versteegh, G.J.M., Bogus, K., Bonnet, S., Bouimetarhan, I., Crouch, E., de Vernal, A., Elshanawany, R., Edwards, L., Esper, O., Forke, S., Grøsfjeld, K., Henry, M., et al., 2013, Atlas of modern dinoflagellate cyst distribution based on 2405 data points: Review of Palaeobotany and Palynology, v. 191, p. 1–197, doi: 10.1016/j.revpalbo.2012.08.003.

1218

Figures main text

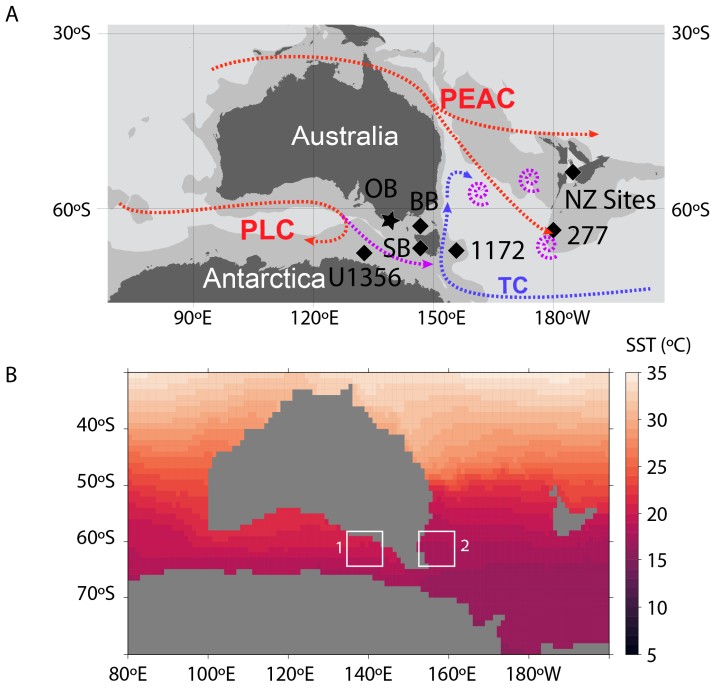

Figure 1. Paleogeographical reconstruction of the Tasman Gateway area around 56 Ma (Müller et al., 2019). **A.** Location of Point Margaret and Latrobe-1 (star) and previously used sites (diamonds) for which data was generated and compiled, respectively. Abbreviations: OB = Otway Basin: Point Margaret and Latrobe-1. BB = Bass Basin (Konkon-1, Poonboon-1), SB=Sorrell Basin (Lowana Road), Tasmania, U1356 = IODP Site U1356, 1172 = ODP Site 1172, 277 = DSDP Site 277, NZ Sites = multiple sites in New Zealand (Mid-Waipara, Tora, Tawanui, Otaio River). For modern locations see Fig. S1. Other abbreviations: PLC = Proto-Leeuwin Current, TC = Tasman Current, PEAC = Proto East Australia Current. Biogeography and simplified model-based currents; red, purple and blue arrows indicate low-latitude, transitional and Antarctic-derived surface currents and eddies, respectively (Bijl et al., 2013a; Sauermilch et al., 2019; Nooteboom et al., 2021). **B.** Regional modeled sea surface temperature. Model run represents a high pCO_2 (6x pre-industrial pCO_2) of CESM1.2 (Zhu et al., 2019; Lunt et al., 2021). Note higher SST in the AAG (box 1) compared to the SW Pacific (box 2) at the same latitude.

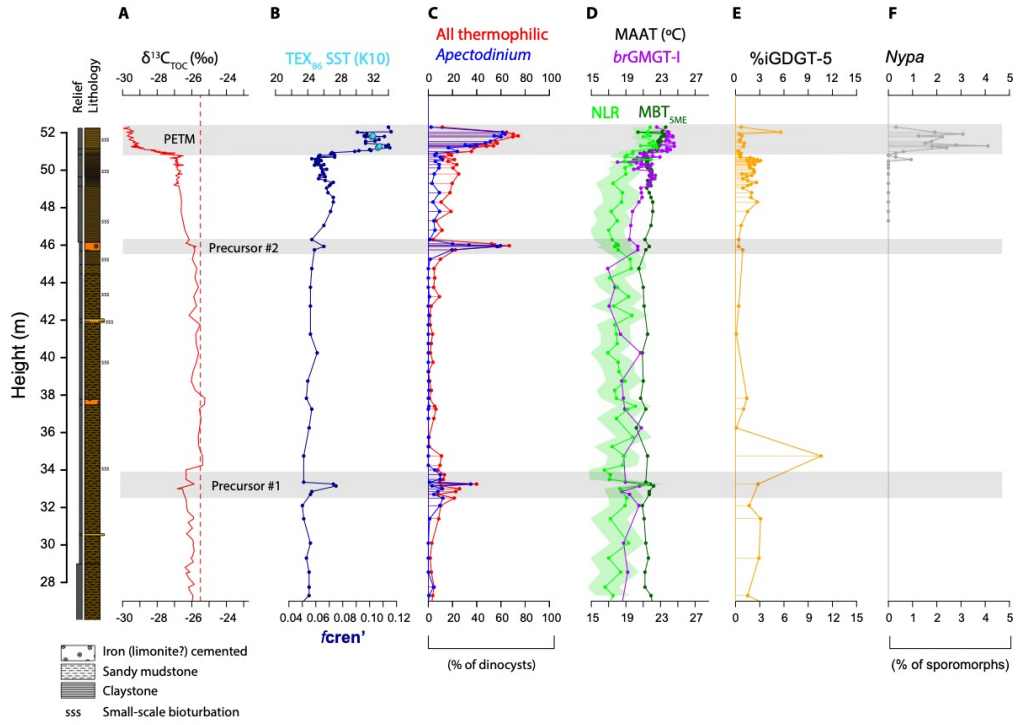

Figure 2. Point Margaret late Paleocene and PETM proxy data. A. Biostratigraphy, bulk organic matter carbon isotope values ($\delta^{13}C_{TOC}$) and lithology from Frieling et al., (2018). **B.** SST trends from relative abundance of crenarchaeol stereoisomer to total crenarchaeol (f(cren'), this study) and TEX_{86}-based SST estimates. Note that the TEX_{86} dataset contains only 4 samples within the PETM CIE. **C.** %*Apectodinium* and %Thermophilic taxa of total dinocyst assemblage (this study). **D.** MAAT estimates based on MBT'_{5Me}, NLR (Huurdeman et al. 2021 & this study), and brGMGTI (this study). **E.** %GDGT-5 (this study). **F.** %*Nypa* of total pollen and spore assemblage (Huurdeman et al. 2021).

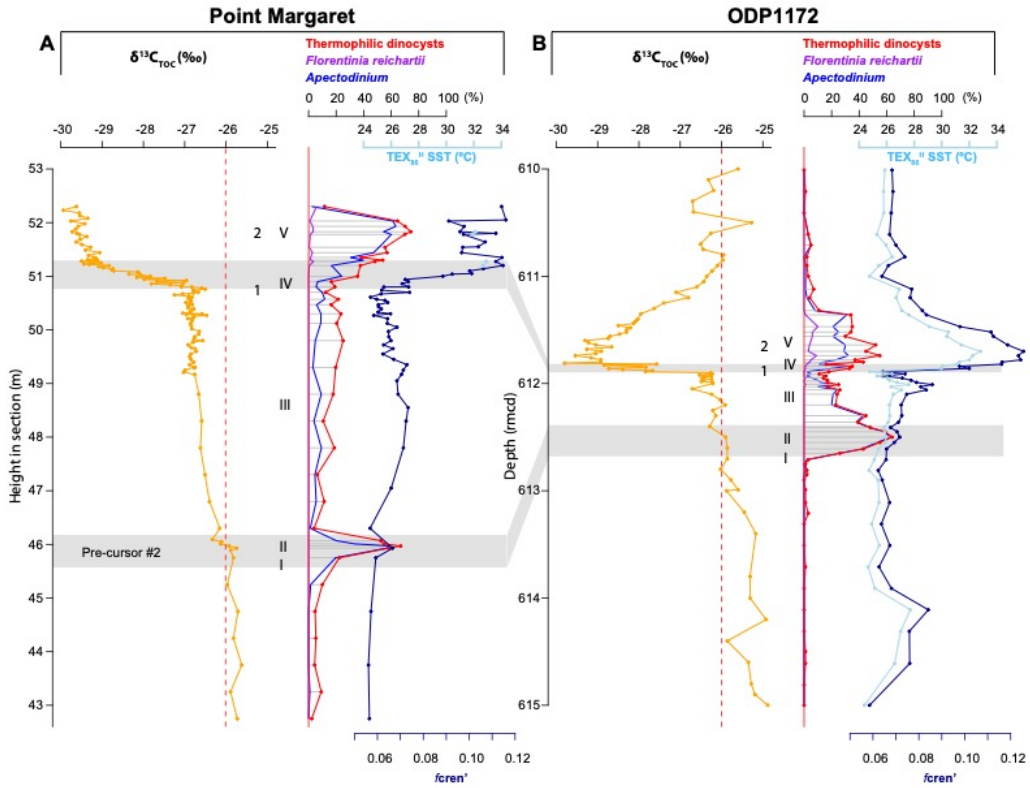

Figure 3. Comparison of latest Paleocene - PETM temperature trends west and east of the Tasman Gateway A. Point Margaret. B. ODP Site 1172. Numbers and roman numerals next to isotope ($\delta^{13}C_{TOC}$) and dinocyst records refer to here correlated events: 1. Onset of the carbon isotope excursion. 2. Body of the carbon isotope excursion. I. Abundance of *Areoligera* complex. II. Abundance (acme) *Apectodinium*. III. Interval with common *Apectodinium*. IV. Abundance (acme) of *Apectodinium*. V. First consistent occurrence of *Florentinia reichartii*. Note that SST at Point Margaret is represented by only 4 TEX_{86} estimates, and limited to the body of the CIE.

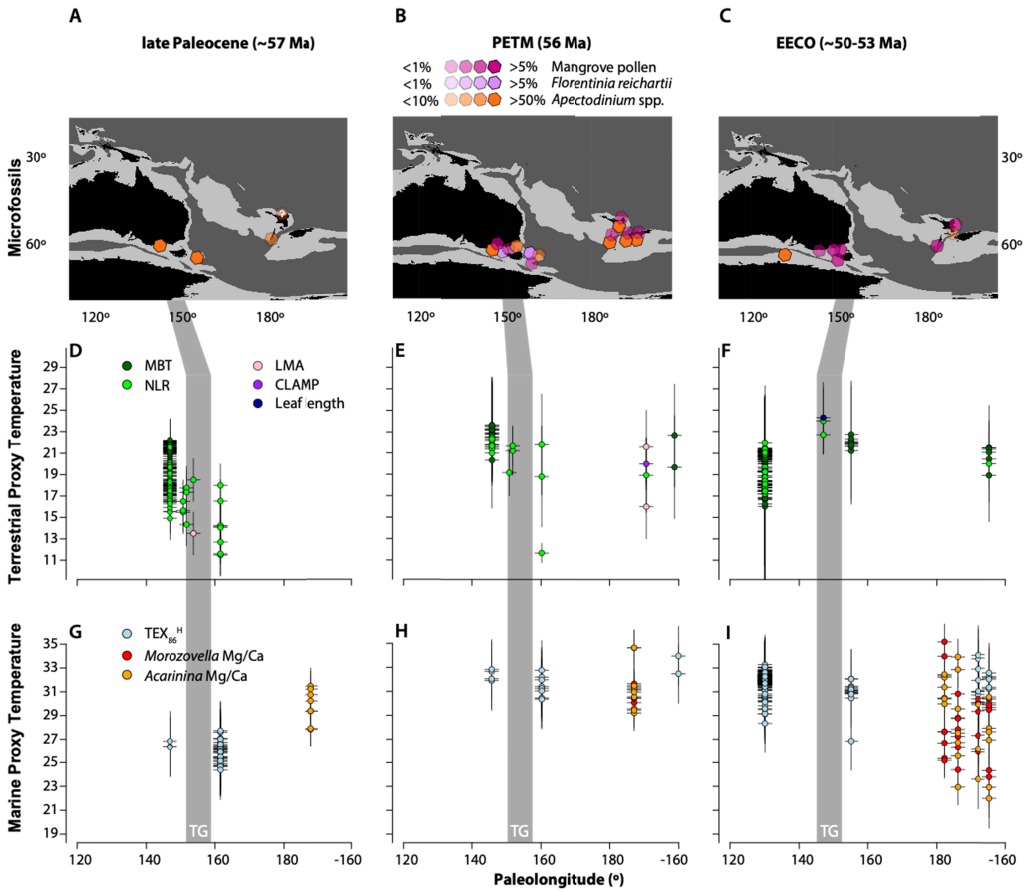

Figure 4: Proxy compilation across three time-slices; late Paleocene, PETM and EECO. A-C. Relative abundance of thermophilic microfossil taxa, mangrove pollen (*Nypa*) and dinocysts (*Apectodinium* and *Florentinia reichartii*), **D-F.** Terrestrial temperature reconstructions based on vegetation (dark green) and biomarkers (green). **G-I.** Sea surface temperature reconstructions using TEX_{86}^{H} (light blue), Mg/Ca of mixed-layer foraminifera *Acarinina* (orange) and *Morozovella* (red). Grey vertical band represents the Tasman Gateway (TG) area.

SST Proxy estimates			late Paleocene			PETM			EECO			
Region	Site	Proxy	n=	mean	SE	n=	mean	SE	n=	mean	SE	Reference
SW Pacific	ODP1172	TEX86H	30	25.9	0.2	8	31.5	0.3	15	30.9	0.3	Bijl et al. 2009, 2013, 2021, Sluijs et al. 2011
		TEXLIN	30	27.2	0.2	8	35.1	0.6	15	34.2	0.5	
	Mid-Waipara	TEX86H				2	33.2	0.8	5	31.6	0.3	Pancost et al. 2013, Hollis et al. 2012
		TEXLIN							5	35.3	0.5	
		Mg/Ca Acarinina							4	26.3	1.3	
	Hampden Beach	TEX86H							8	31.9	0.5	Hollis et al. 2009, Hines et al. 2017, Inglis et al. 2015
		TEXLIN							8	35.9	0.8	
		Mg/Ca Morozovella							5	28.6	0.9	
		Mg/Ca Acarinina							3	26.6	1.8	
	DSDP277	Mg/Ca Morozovella				7	31.4	0.6	5	29.3	1.4	Hollis et al. 2015, Hines et al. 2017
		Mg/Ca Acarinina	8	29.8	0.5	8	30.9	0.6	6	31.2	0.4	
	Tora	Mg/Ca Morozovella							6	25.7	0.9	Hines et al. 2017
		Mg/Ca Acarinina							6	26.8	1.7	
	Tawanui	Mg/Ca Morozovella							1	27.2		Hines et al. 2017
		Mg/Ca Acarinina							1	25.6		
Australo-Antarctic Gulf	U1356A	TEX86H							131	31.9	0.1	Bijl et al. 2013
		TEXLIN							131	35.7	0.1	
	Latrobe-1	TEX86H	2	27.3	0.2							This study
		TEXLIN	2	29	0.3							
	Point Margaret	TEX86H	1	26.3		4	32.4	0.2				This study
		TEXLIN				4	36.5	0.4				

MAAT Proxy estimates			late Paleocene			PETM			EECO			
Region	Site	Proxy	n=	mean	SE	n=	mean	SE	n=	mean	SE	Reference
SW Pacific	ODP1172	MBT							9	21.9	0.1	Bijl et al. 2013, 2021
		WLR	8	14.1	0.8	3	17.4	3.0				Contreras et al. 2014
	Mid-Waipara	MBT				2	21.2	1.5	6	20.8	0.4	Pancost et al. 2013
		Coexistence							1	20.0		
	Konkon-1	WLR	3	16.5	1.1	2	21.4	0.2				Contreras et al. 2014
	Poonboon-1	WLR	3	15.9	0.3	1	19.2					Contreras et al. 2014
	Cambalong creek	WLR	1	18.5								Greenwood et al. 2003, Contreras et al. 2014
		LMA	1	13.5								
Australo-Antarctic Gulf	Point Margaret	WLR	66	17.9	0.2	8	21.7	0.2				Huurdeman et al. 2021 & this study
		MBT	70	21.3	0.1	12	22.9	0.3				Huurdeman et al. 2021 & this study
		brGMGT-I	***58***	***19.7***	***0.2***	12	23.6	0.2				This study
	Latrobe-1	WLR	6	19.7	0.1	1	22.3					This study
	U1356A	MBT							62	20.1	0.2	Pross et al. 2012
		WLR							81	18.4	0.1	
	Lowana Road, Tasmania	Coexistence							2	23.4	0.7	Carpenter et al. 2012
		Podocarpus leaf length							1	24.3		
		WLR							1	20.0		Reichgelt et al. 2022
	Deans Marsh	CLAMP							1	22.6		Reichgelt et al. 2022
		WLR							1	19.5		Reichgelt et al. 2022
	Dinmore	CLAMP							1	19.7		Reichgelt et al. 2022
		WLR							1	18.9		Reichgelt et al. 2022

Semi-quantitative temperature estimates			late Paleocene	PETM	EECO	
Region	Site	Proxy	minimum	minimum	minimum	Reference
SW Pacific	ODP1172	Dinocysts	20	25	25	Sluijs et al. 2011, Bijl et al. 2021
		Pollen		22		Contreras et al. 2014
	Mid-Waipara	Dinocysts		20		Crouch et al. 2014 & references therein
	Tawanui	Dinocysts		20		Crouch et al. 2014 & references therein
	Kumara-2	Dinocysts		20		Crouch et al. 2014 & references therein
	Toi-Flat-1	Dinocysts		20		Crouch et al. 2014 & references therein
Australo-Antarctic Gulf	Point Margaret	Dinocysts	20	25		This study
		Pollen		22		Huurdeman et al. (2021)
	Latrobe-1	Dinocysts	20	25	20	This study
		Pollen		22	22	This study
	Lowana Road, Tasmania	Pollen & Macrofossils			22	Carpenter et al. 2012
	U1356A	Dinocysts			20	Bijl et al. 2013

Table 1. From top to bottom - SST, MAAT and semi-quantitative minimum temperature proxy estimates for the SW Pacific and AAG. Data sources: (Greenwood et al., 2003; Bijl et al., 2009; Hollis et al., 2009; Sluijs et al., 2011; Carpenter et al., 2012; Hollis et al., 2012; Pross et al., 2012; Bijl et al., 2013a; Pancost et al., 2013; Contreras et al., 2014; Crouch et al., 2014; Hollis et al., 2015; Inglis et al., 2015; Hines et al., 2017; Bijl et al., 2021; Huurdeman et al., 2021; Reichgelt et al., 2022)

Figure 1.

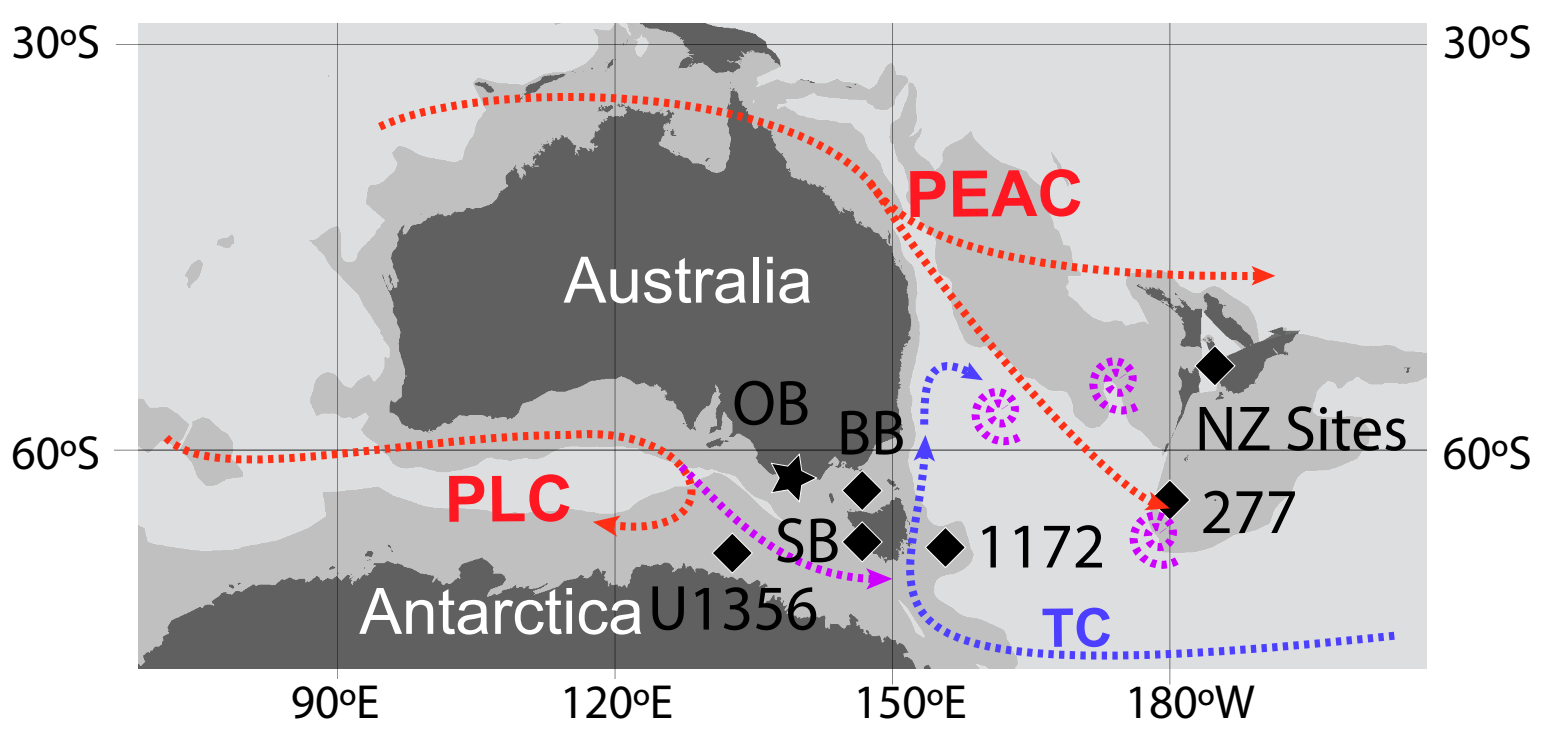
30°S
30°S
60°S
60°S
PEAC
Australia
OB
BB
NZ Sites
PLC
277
SB
1172
Antarctica
U1356
TC
90°E
120°E
150°E
180°W

Figure 2.

A
B
C
D
E
F
$\delta^{13}C_{TOC}$ (‰)
TEX_{86} SST (K10)
All thermophilic
Apectodinium
MAAT (ºC)
*br*GMGT-I
NLR
MBT_{5ME}
%iGDGT-5
Nypa
Relief
Lithology
PETM
Precursor #2
Precursor #1
Height (m)
52
50
48
46
44
42
40
38
36
34
32
30
28
sss
-30 -28 -26 -24
20 24 28 32
0 20 40 60 80 100
15 19 23 27
0 3 6 9 12 15
0 1 2 3 4 5
0.04 0.06 0.08 0.10 0.12
*f*cren'
(% of dinocysts)
(% of sporomorphs)
Iron (limonite?) cemented
Sandy mudstone
Claystone
sss Small-scale bioturbation

Figure 3.

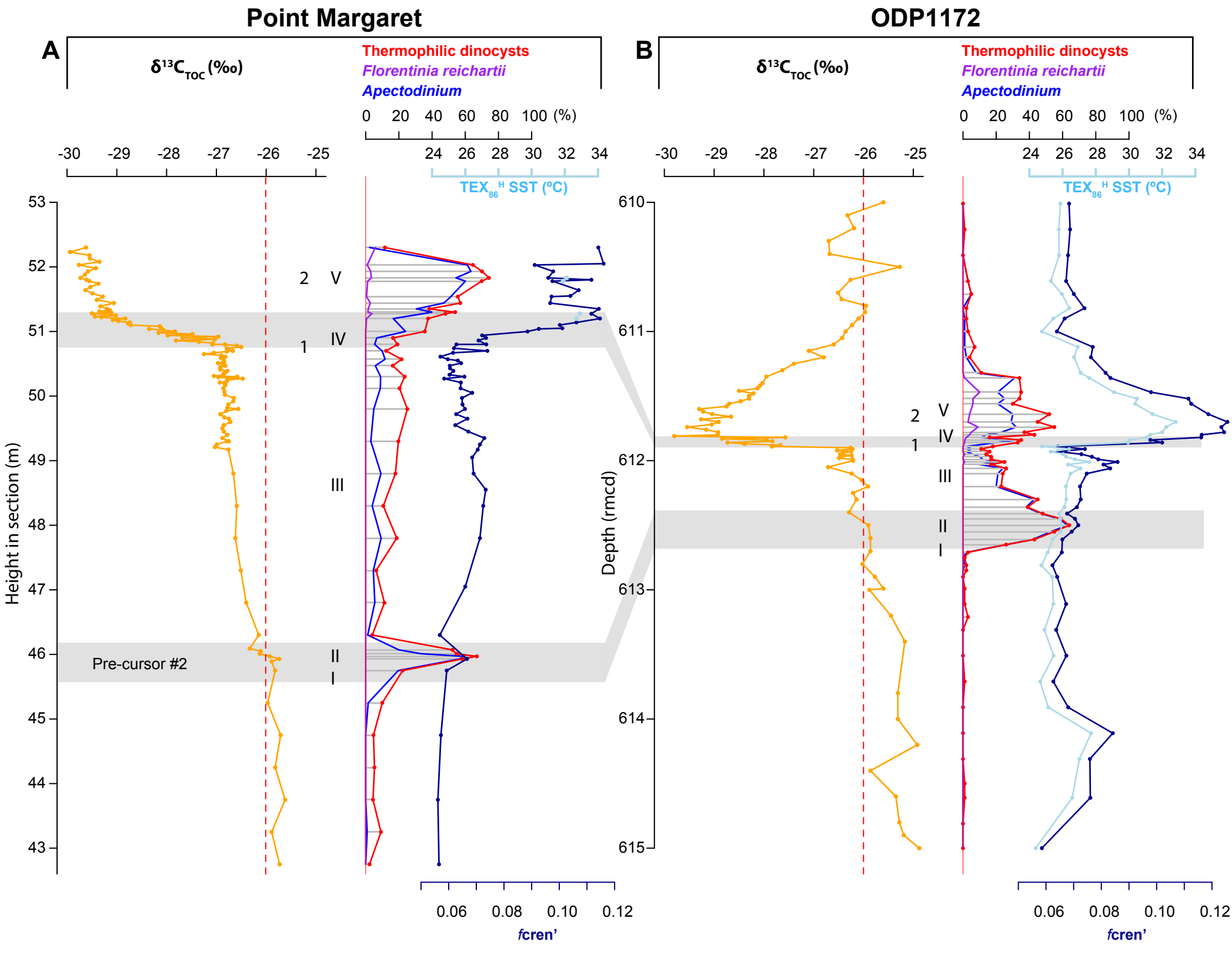
Point Margaret
ODP1172
A
B
δ13CTOC (‰)
Thermophilic dinocysts
Florentinia reichartii
Apectodinium
0 20 40 60 80 100 (%)
-30 -29 -28 -27 -26 -25
24 26 28 30 32 34
TEX86H SST (ºC)
Height in section (m)
Depth (rmcd)
53 52 51 50 49 48 47 46 45 44 43
610 611 612 613 614 615
2 V
1 IV
III
II
I
Pre-cursor #2
0.06 0.08 0.10 0.12
fcren'

Figure 4.

A

late Paleocene (~57 Ma)

B

PETM (56 Ma)

C

EECO (~50-53 Ma)

<1% >5% Mangrove pollen
<1% >5% *Florentinia reichartii*
<10% >50% *Apectodinium* spp.

Microfossils

30°
60°

120° 150° 180°

D

E

F

Terrestrial Proxy Temperature

MBT
NLR
LMA
CLAMP
Leaf length

29 27 25 23 21 19 17 15 13 11

G

H

I

Marine Proxy Temperature

TEX_{86}^{H}
Morozovella Mg/Ca
Acarinina Mg/Ca

35 33 31 29 27 25 23 21 19

TG

120 140 160 180 -160

Paleolongitude (°)

Supplementary Text

Dinocyst assemblages

Point Margaret

Overall, latest Paleocene dinocyst assemblages (Fig. S8) at Point Margaret are entirely dominated by small Peridinioid taxa, including *Spinidinium*, *Vozzhennikovia*, *Phthanoperidinium* and *Senegalinium*. This suggests a strong fresh-water influence, in line with the general lithological evolution of the site that suggests a trend from high-energy sand dominated facies to silt and mud-dominated pro-delta deposits (Frieling et al., 2018). Across the condensed interval at ~46m open marine taxa (*Spiniferites*, *Cordosphaeridium*, *Glaphyrocysta* and *Apectodinium*) are temporarily abundant, signaling continuous marine influence. At the onset of the CIE, the abundance of *Apectodinium* spikes again, reaching maximum abundance of *ca.* 60% of the assemblage. *Florentinia* consistently occurs within the topmost part of the section, at the body of the CIE. The general assemblage characteristics and evolution, with e.g. the abundant low-salinity tolerant small Peridinioid taxa and a distinct pre-PETM *Apectodinium* abundance are strongly reminiscent of the assemblages at ODP 1172 (Sluijs et al., 2011) and several events can be correlated (Figure 3).

Latrobe-1

Much of the trends observed at Point Margaret are observed in the Latrobe-1 material as well (Fig. S9), but the dominance of the small Peridinioids is less pronounced and dinocyst concentrations are generally much lower (Frieling et al., 2018). The reduced abundance was previously hypothesized to result from long-term storage (Frieling et al., 2018). Similarly, Peridinioids may be disproportionately affected by this degradation, compared to Gonyaulacoid cysts (e.g. Zonneveld et al., 2019, 2008). We argue this also plays a role in shaping the dinocyst assemblages at Latrobe-1. During the PETM, *Apectodinium* is extremely abundant, with ca. 90% of the assemblage, but *Florentinia* is represented by only a single specimen. Based on the CIE profile, the highest abundance of *Apectodinium* is likely positioned above the top of the Point Margaret outcrop and is therefore missing.

Supplementary Figures

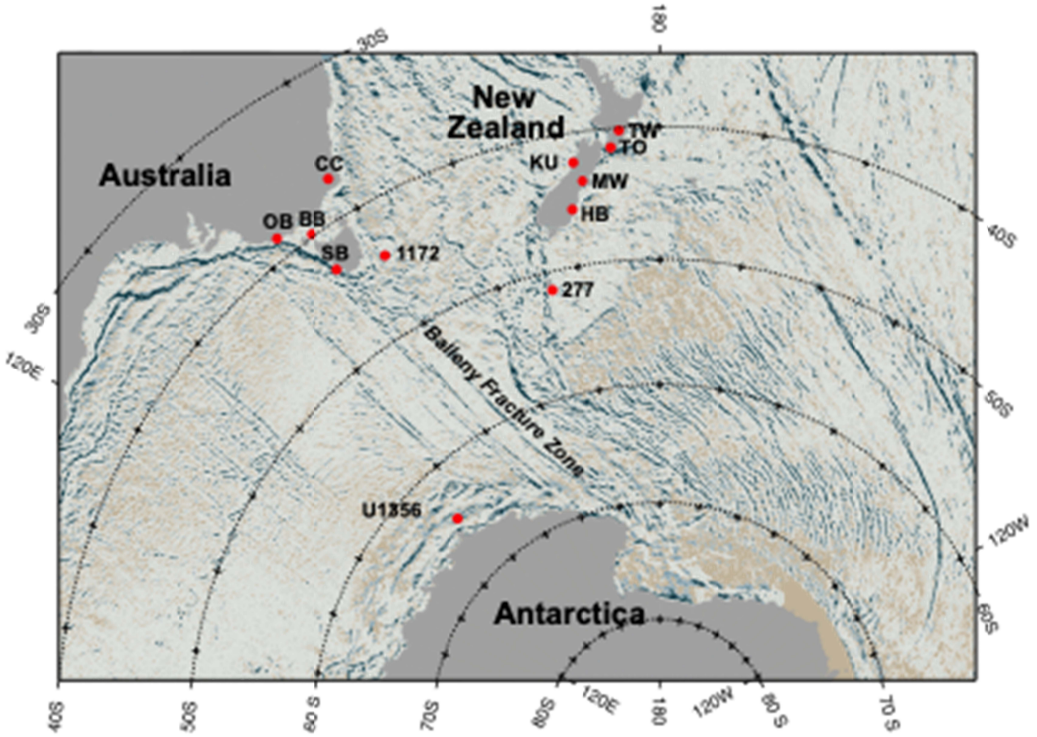

Figure S1. Modern distribution of localities used in this study. Abbrevations & numbers as follows: Cambalong Creek (CC), Otway Basin (OB), Bass Basin (BB), Sorrell Basin (SB), Kumara core (KU), Hampden Beach (HB), Mid-Waipara river (MW), Tora (TO), Tawanui (TW) and numbered Deep Sea Drilling Project (DSPD) Site 277, Ocean Drilling Program (ODP) Site 1172 and Integrated Ocean Drilling Program (IODP) Site U1356.

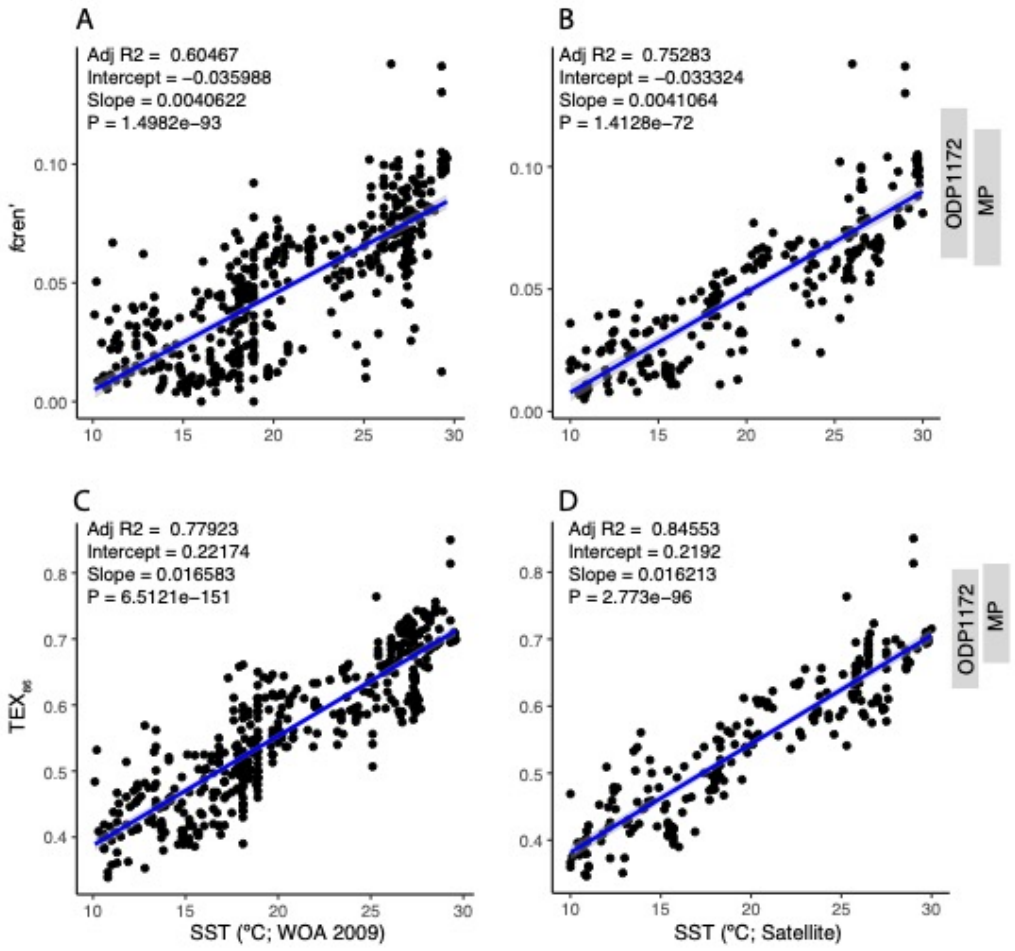

Figure S2. Linear correlations of cren'/total crenarchaeol (f(cren')) and TEX_{86} with SST (>10°C and no Red Sea) in two widely used calibration datasets; Kim et al. 2010 (K2010)(Kim et al., 2010) **and the more expanded Tierney & Tingley 2015 (TT2015)** (Tierney and Tingley, 2015)**.** A. f(cren') in TT2015. B. (fcren') in K2010. C. TEX_{86} vs SST in TT2015. D. TEX_{86} vs SST in K2010. Bars on the right represent the range of observed values for the Paleocene and PETM in the Point Margaret outcrop and Latrobe-1 (MP) and Site 1172 cores. Note that there are only 5 reliable TEX_{86} datapoints in the Point Margaret and 2 in Latrobe-1.

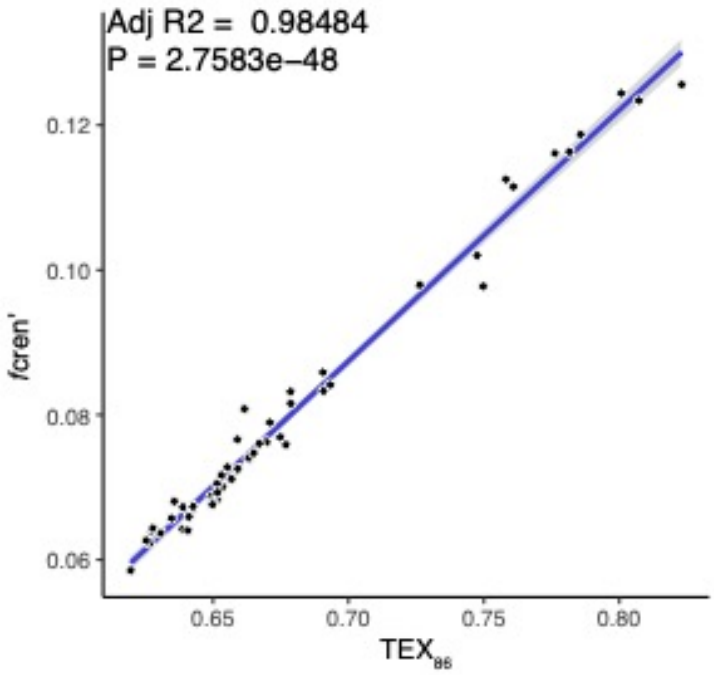

Figure S3. Linear correlation between TEX_{86} and *f*cren' at ODP Site 1172 across the PETM.

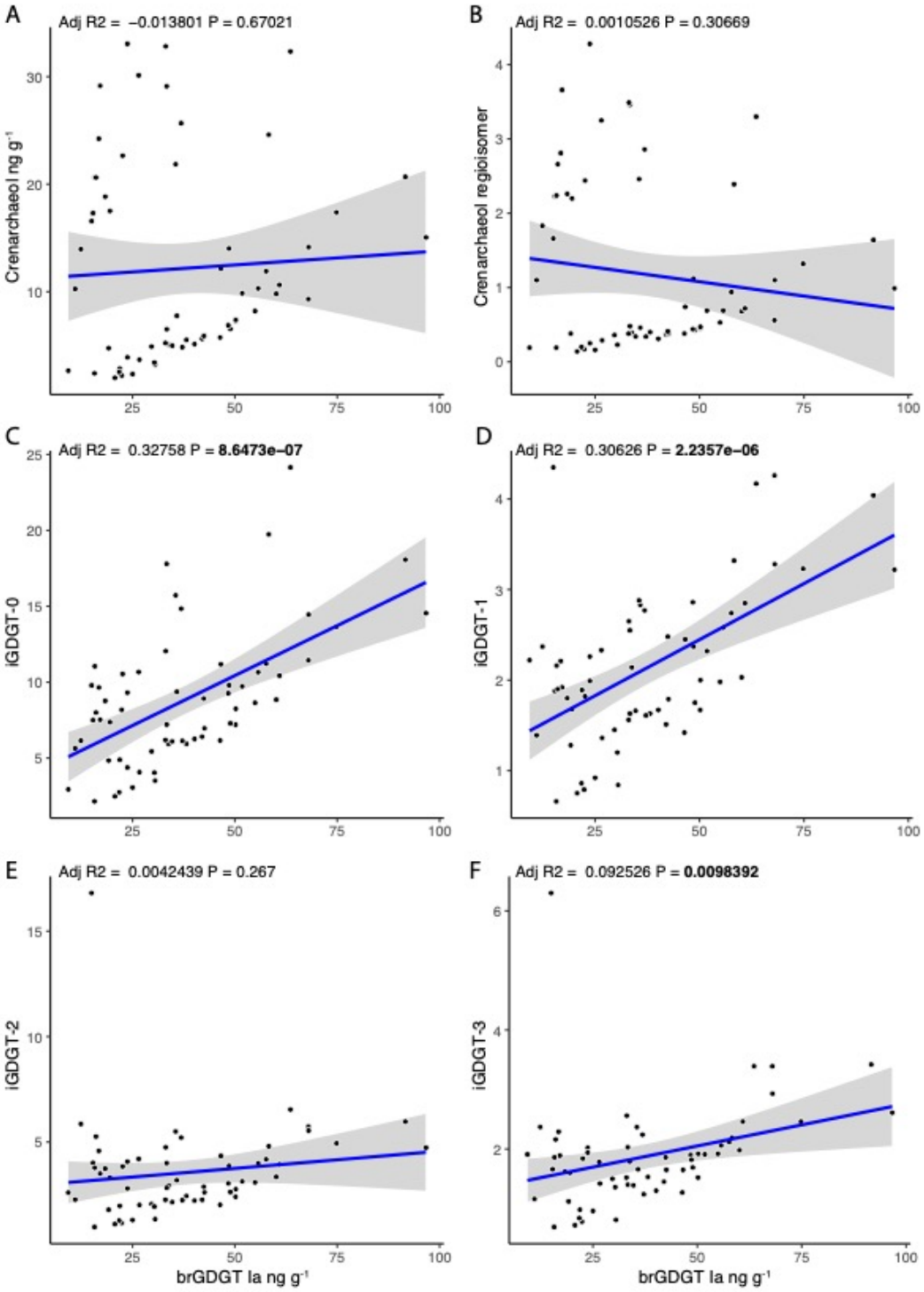

Figure S4. Absolute abundances of individual isoprenoid GDGTs compared to abundance of the predominant branched GDGT-Ia in ng g^{-1} dry sediment. A. Crenarchaeol, B. Crenarchaeol isomer, C. GDGT-0, D. GDGT-1, E. GDGT-2, F. GDGT-3. Note that GDGT-0, 1 and 3 show a significant correlation ($P < 0.01$). Units on all axes are measured concentrations.

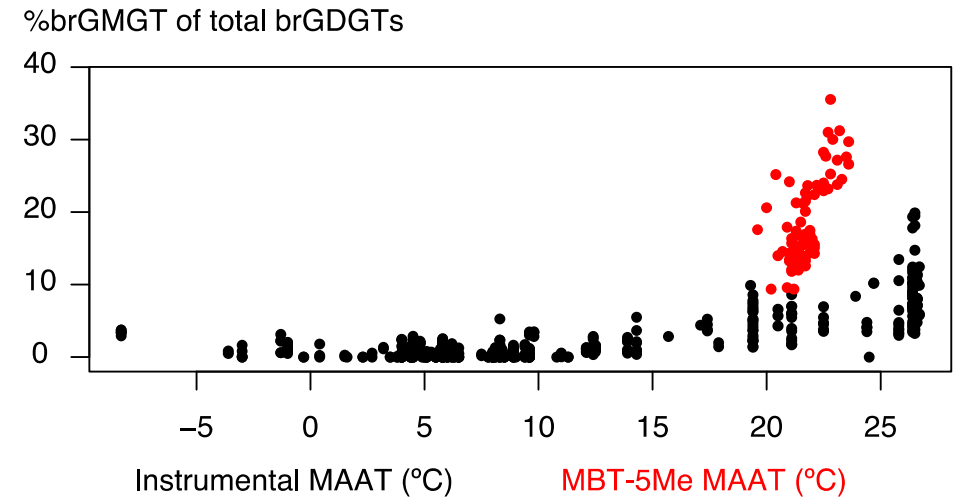

Figure S5. Abundance of brGMGTs as percentage of total brGMGTs + brGDGTs (%brGMGT). Black dots represent the modern peat database (Naafs et al., 2018), red dots represent the late Paleocene – PETM at Point Margaret (this study). Both datasets are compared to MAAT, which was measured and reconstructed using MBT'$_{5Me}$, for the modern and ancient data, respectively.

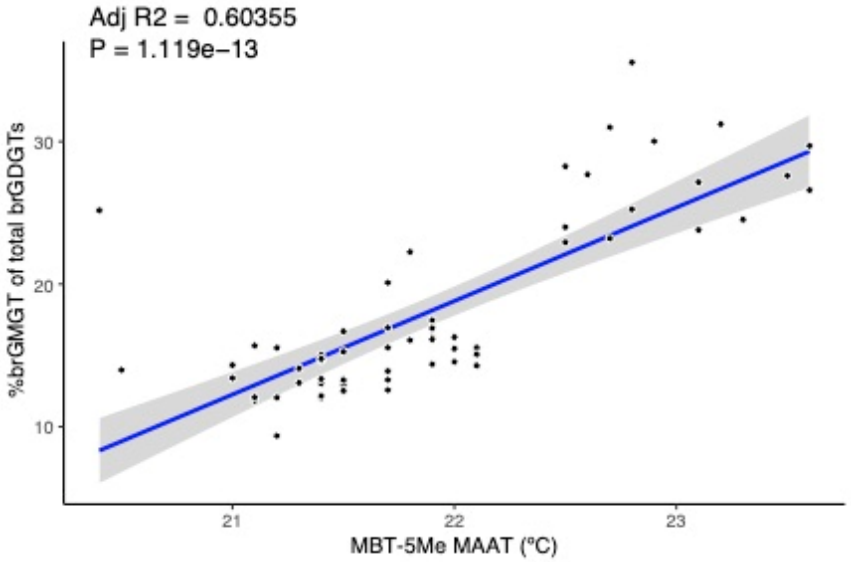

Figure S6. Correlation between %brGMGTs and MBT'$_{5Me}$ derived MAAT at Point Margaret.

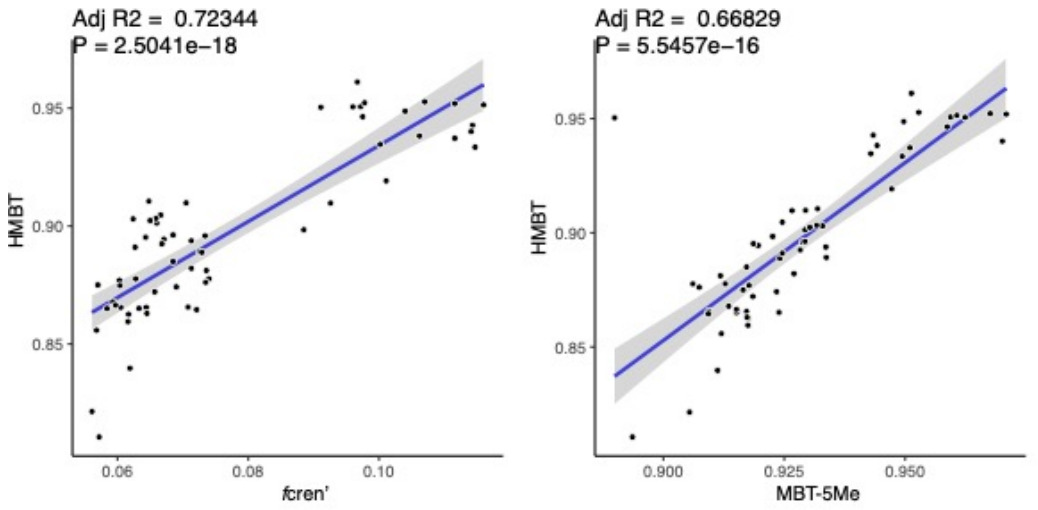

Figure S7. Correlation of HMBTacyclic to other lipid biomarker proxies; fcren' and MBT'$_{5Me}$

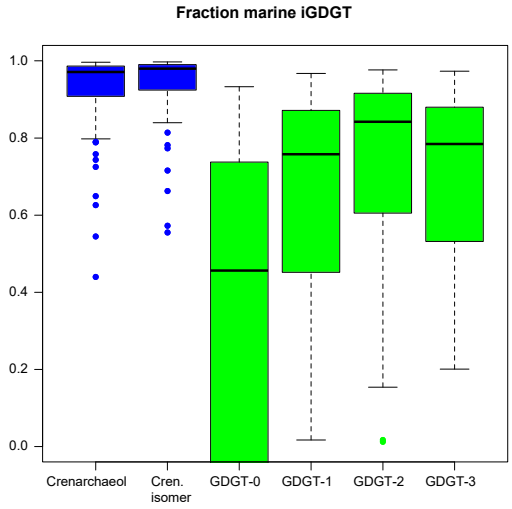

Figure S8. Average amount of marine contribution to the iGDGT-pool calculated following methods described in Sluijs et al., (2020)**.** The terrestrial fraction in isoGDGT-0 is potentially dominant over the marine in the majority of samples, whereas crenarchaeol and the stereoisomer remain almost exclusively marine.

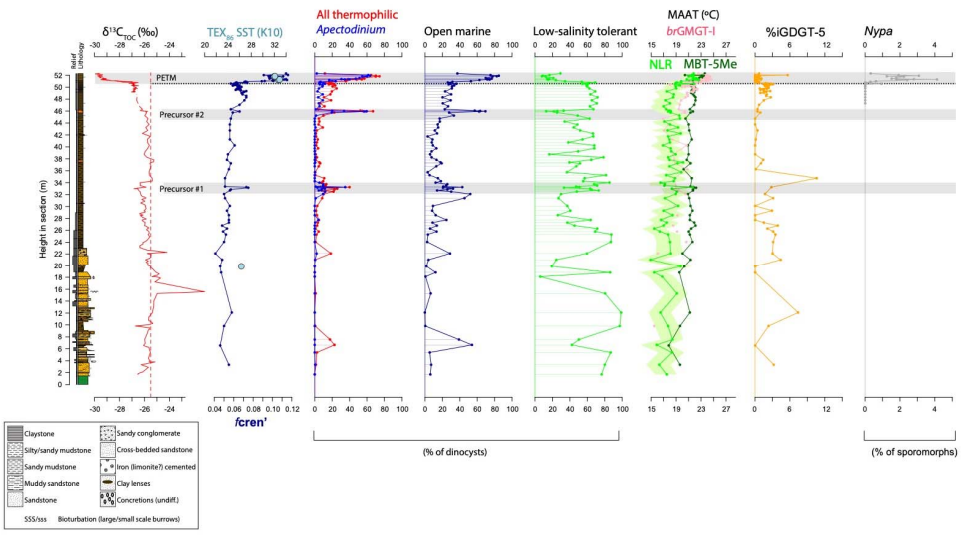

Figure S9. Ecological signals based on dinocyst assemblages, pollen and lipid biomarker proxy data for the entire Late Paleocene and PETM succession at Point Margaret. Interpretation follows ecological preferences of Frieling & Sluijs (2018; and references therein). See SI data for grouping.

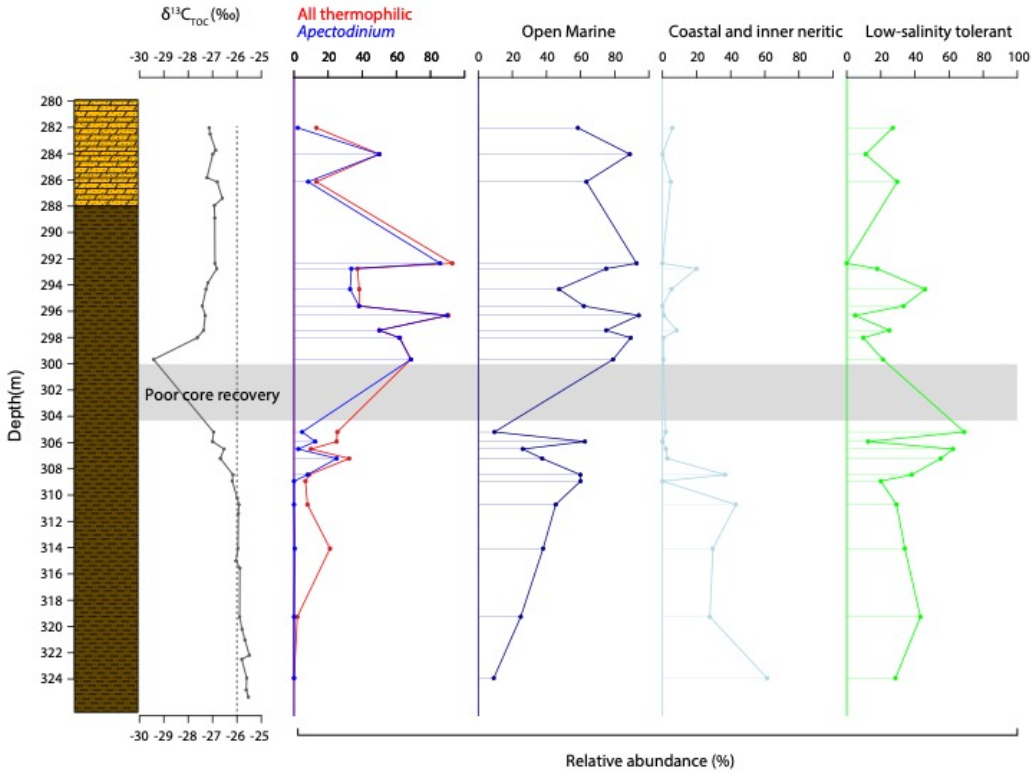

Figure S10. Ecological signals based on dinocyst assemblages for Latrobe-1 across the PETM. Interpretation follows ecological preferences of Frieling & Sluijs (2018; and references therein). See SI data for grouping.